Corso di Laurea Magistrale in Ingegneria Aerospaziale

POLITECNICO
DI TORINO

Multiphase simulations for vehicle external water management

Relatore:
Prof. Michele Iovieno

Correlatore:
Ing. Laura Maria Lorefice

Candidato:
Matteo Allocco

Anno accademico 2017/2018
March 14, 2018

Ringraziamenti

Desidero ringraziare FCA Italy e l'Ing. Laura Maria Lorefice per l'opportunità di apprendimento che mi hanno offerto. Un grazie anche all'Ing. Paola Nicola e all'Ing. Piovano Andrea Alessandro di FCA Italy che mi hanno seguito personalmente durante lo svolgimento di questa tesi. Un ulteriore ringraziamento anche a Simone Landi di Siemens, che ha fornito il suo prezioso supporto tecnico relativo al software STAR-CCM+ in alcuni momenti critici. Esprimo ancora la mia gratitudine verso lo staff di FCA - Aerothermal PCC, che ha sempre saputo alleviare mio tempo trascorso nel suo ufficio.

Ringrazio il Prof. Michele Iovieno per i suoi consigli e per l'attenzione dedicatami.

Infine un ringraziamento alla mia famiglia per costante supporto che mi ha sempre fornito.

Contents

Chapter 1

Introduction

With the technological progress of the last few decades, the automotive industry took several steps forward in terms of performances, efficiency and safety of cars. These improvements were possible thanks to the increase in reliability and accuracy of the numerical and experimental engineering techniques. This technological development led car companies to set higher targets that in the past were unreachable. A consequence of the development of engineering solutions is represented by the birth of even stricter regulations, that affected an even wider number of components of the car, making what once was a secondary feature of the project, now highly important for its success. In particular, success is not intended only in engineering terms, but also in terms of sales and customer satisfaction.

The topic of this document will be an example of what just stated. In the field of fluid dynamics, numerical methods and mathematical models to whom the first are applied saw a strong increase of their usage in the last decades. A reason for this fact lies the steps made in the field of computer science and parallel computing. They allowed to reduce calculation times and reach a relevant precision in the numerical results, included those whose experimental validation would be hard and expensive to obtain.

1.1 Water management

The current thesis will focus on one of the topics that current engineering methodologies in the automotive field are now able to face: the *water management*, i.e. determining the behaviour of water droplets around the vehicle and on its surfaces in rainy conditions. In particular, two phenomena that happen when driving in the rain or in truck wakes in rainy days will be investigated:

- *water soiling* on the side glasses, i.e. how these ones are wetted by rain. In particular a comparison between different strategies to investigate this phenomenon is made. An effort will be made to understand how the shapes of the A-pillar and the rear-view mirror affect this phenomenon.
- *water ingestion* inside the engine intake system. A way to numerically replicate a wind tunnel test will be proposed. The purpose of this wind tunnel test is to check whether rain water affects the engine performance or not.

All the tasks will be developed at FCA Aerothermal PCC Departement located in Orbassano (Turin). Where possible, then, the results of numerical simulations will be compared to those obtained in the FCA's climatic wind tunnel. The vehicle analysed will always be the Jeep Renegade.

With the purpose of running the mentioned analysis, a massive use of CFD (Computational Fluid Dynamics) simulations will be made. In particular the commercial software STAR-CCM+ 10.06.009 will be used. In facts, it includes all the physical models known at the moment that can be used to describe a multiphase flow. In particular there are several models that can be applied to the cases mentioned above and they will all be considered and compared. The computational power is as well given by FCA's cluster.

1.1.1 Soiling

The soiling phenomenon , i.e. the accumulation of water or small debris on the surface of the vehicle, can result to be very dangerous when these surfaces are the car glasses. In fact, external visibility is a crucial point for the driver of the vehicle: if it gets even partially compromised, the driver could be affected in terms of longer response times to an obstacle or a pedestrian, for example. Secondary issues linked to soiling phenomena are then the dimming of the cameras, such as those used for parking, and the contamination of the people who get in contact with the soiled surfaces. As mentioned before, this part will focus on side windows soiling and how this phenomenon is affected by the rear view mirrors and the A-pillar.

Soiling is a topic whose investigation is usually quite inaccurate because of the several degrees of freedom that are involved. A correct mathematical model of rain takes into account variables such as the droplets diameter, their direction and velocity with respect to the car and to the wind, the intensity of rain, an eventual preceding car, and so on. When this problem will be faced, in the next chapters, some assumptions will necessarily be made. Lateral visibility in rain conditions, because of the complexity of finding an accurate model for the rain, is one of those fields that still lies outside of the regulation and that is still somehow neglected by the common standardized engineering procedures, whose aim is to succeed in the approval tests of the vehicle.

The purpose of this section is therefore to compare different multiphase currently existing models that are implemented in the commercial software STAR-CCM+ and that can be applied to this issue. Between them the most reliable will be the one that gets closer to the few experimental data available. More in details, the models compared are mainly two: the first one is based on the Eulerian formulation of the Navier-Stokes equations, while the second one is based on the Lagrangian point of view of the water droplets.

1.1.2 Water ingestion

The second part will focus on the behaviour of the water that gets into the engine air aspiration duct. Common external aerodynamics CFD simulations see the engine aspiration system as an outlet whose air mass flow exiting the fluid domain is imposed as a boundary condition. Here the domain will be extended beyond this limit and will include all the the aspiration duct and its filter. In this way, using the same models that were used for soiling simulations, the amount of water that actually reaches the engine and that could affect the combustion can be measured.

The results will be compared with the experimental ones that were obtained in the wind tunnel following the rules of the Slipstream test. In fact, a practical test has to be done: the vehicle is exposed to the wind in a wind tunnel at a certain velocity for a certain time interval and a well determined water mass flow is sprayed on front of it. At the end of the test the engine filter is dismounted and weighted: the extra weight is therefore that of the ingested water. In order for the test to be successful, this amount of water must be under a specific limit. The task of the CFD simulations is then to achieve the same results as those obtained in the wind tunnel and so to be a reliable numerical tool to predict the result of the test.

Figure 1.1: The Jeep Renegade

Chapter 2

Numerical simulations

In the first section of this chapter the governing equations of fluid dynamics are reported and briefly commented, since they will always be solved in every CFD simulation. Then the next sections will deal with some different approaches used in turbulence modelling. A section regarding the solution algorithm will follow, and then the space discretization will be described in the last part, as it is a fundamental operation to be done in order to reach an accurate solution. The very last section deals with porous media models.

2.1 Governing equations: Eulerian and Lagrangian formulation

As far as fluid dynamic is concerned, it is nowadays proved that all of its features are well described by the conservation equations (also known as the Navier-Stokes equations). Basically they state that, in a fluid continuum, mass, momentum and energy are conserved. They will be briefly reminded and commented in the next subsections. Before proceeding, though, it is convenient to point out the difference between the meaning of a common local derivative and the total (or substantial) derivative. If the derivative operations of a variable (such as the density ρ, for example) is made with respect to time t, then the local derivative shows how this variable varies in time in a fixed point in space, while the substantial derivative shows how it changes following a single fluid particle that moves in space and time. The total derivative is also referred to as the Lagrangian derivative and is defined as:

$$\frac{D(.)}{Dt} = \frac{\partial(.)}{\partial t} + (\mathbf{V} \cdot \nabla(.)) \tag{2.1}$$

where, in the right hand term, the first part is the local derivative (i.e. for a fixed point in space) and the second one is the convective derivative (the time rate of change due to the movement of the observed fluid particle).

2.1.1 The continuity equation

One of the fundamental laws of fluid dynamics is the mass conservation equation, also known as the continuity equation. Given an arbitrary finite volume of fluid, fixed in space, this equation states that the net mass flow out of the control volume trough its surface is equal to the time rate of decrease of mass inside the control volume. If this volume is infinitesimally small, the equation can be written in the following way:

$$\frac{\partial\rho}{\partial t} + \nabla \cdot (\rho\mathbf{V}) = 0 \tag{2.2}$$

where ρ is the fluid density, $\mathbf{V}$ is the velocity vector (whose components are u, v and w)and t is time. What's more, this is called the *conservation form* of the equation, because it refers to a fixed volume of fluid in space. Of course, for an incompressible flow (i.e. Mach number lower than 0.3) the previous equation reduces to:

$$\nabla \cdot \mathbf{V} = 0 \tag{2.3}$$

On the other hand, if a small element of constant mass, but variable volume, is followed, the *non-conservation* form of the continuity equation is obtained. It is written in a differential form as well:

$$\frac{D\rho}{Dt} + \rho \nabla \cdot \mathbf{V} = 0 \tag{2.4}$$

Both equations 2.2 and 2.4 are written in partial differential form, but they can easily be manipulated in order to get their integral form, that is used when they have to be applied to a bigger volume. It also has to be said that it is possible to switch from a *conservative* form to a *non-conservative* one trough few operations, as showed by Anderson [1]. In commercial CFD codes, then, the integral form of equation 2.2 is usually solved, but the meaning of the equations that have just been described does not change.

2.1.2 The momentum equation

The momentum equation takes into account all the forces acting on the control volume. In particular it can be seen as another expression for Newton's second law:

$$F = \frac{\partial (mV)}{\partial t} \tag{2.5}$$

where F is the sum of all forces acting on the mass m. The forces that act on the fluid are both body forces (such as gravity) and surface forces (such as pressure forces and shear and normal stresses on the surface of the control volume). In particular the momentum equation states that the sum of the time rate of increase of momentum inside the control volume and the rate of convective out-flux of momentum across the control surface is equal to the sum of body and surface forces. As in the case of the continuity equation, there are a *conservation form* and a *non-conservation form* of the equation, depending on whether the control volume is fixed in space or not. Being a vector equation, the equilibrium has to be satisfied along the three directions, so the momentum equation is actually made of three equations. What follows is their differential conservation form:

$$\frac{\partial (\rho u)}{\partial t} + \nabla \cdot (\rho u \mathbf{V}) = -\frac{\partial p}{\partial x} + \frac{\partial \tau_{xx}}{\partial x} + \frac{\partial \tau_{yx}}{\partial y} + \frac{\partial \tau_{zx}}{\partial z} + \rho f_x \tag{2.6}$$

$$\frac{\partial (\rho v)}{\partial t} + \nabla \cdot (\rho v \mathbf{V}) = -\frac{\partial p}{\partial y} + \frac{\partial \tau_{xy}}{\partial x} + \frac{\partial \tau_{yy}}{\partial y} + \frac{\partial \tau_{zy}}{\partial z} + \rho f_y \tag{2.7}$$

$$\frac{\partial (\rho w)}{\partial t} + \nabla \cdot (\rho w \mathbf{V}) = -\frac{\partial p}{\partial z} + \frac{\partial \tau_{xz}}{\partial x} + \frac{\partial \tau_{yz}}{\partial y} + \frac{\partial \tau_{zz}}{\partial z} + \rho f_z \tag{2.8}$$

where f_i is a generic external force per unit of mass acting on the control volume, while τ_{ij} is the viscous stress defined as (using Einstein's notation):

$$\tau_{ij} = \mu \left(\frac{\partial u_i}{\partial x_j} + \frac{\partial u_j}{\partial x_i} \right) + \delta_{ij} \lambda \nabla \cdot \mathbf{V} \tag{2.9}$$

In equation 2.9 δ_{ij} is the Kronecker delta ($\delta = 1$ for $i = j$, otherwise $\delta = 0$), μ is the fluid molecular viscosity, or dynamic viscosity, and λ is the bulk viscosity. According to Stokes' hypothesis:

$$\lambda = -\frac{2}{3}\mu \tag{2.10}$$

The previous hypothesis is true for all common aerodynamic applications, such as the flow field around a vehicle. Equations 2.6, 2.7, 2.8 are also known as the proper Navier-Stokes equation. From a Lagrangian point of view (*non-conservation form*), momentum conservation is expressed as follows:

$$\rho\frac{Du}{Dt} = -\frac{\partial p}{\partial x} + \frac{\partial \tau_{xx}}{\partial x} + \frac{\partial \tau_{yx}}{\partial y} + \frac{\partial \tau_{zx}}{\partial z} + \rho f_x \tag{2.11}$$

$$\rho\frac{Dv}{Dt} = -\frac{\partial p}{\partial y} + \frac{\partial \tau_{xy}}{\partial x} + \frac{\partial \tau_{yy}}{\partial y} + \frac{\partial \tau_{zy}}{\partial z} + \rho f_y \tag{2.12}$$

$$\rho\frac{Dw}{Dt} = -\frac{\partial p}{\partial z} + \frac{\partial \tau_{xz}}{\partial x} + \frac{\partial \tau_{yz}}{\partial y} + \frac{\partial \tau_{zz}}{\partial z} + \rho f_z \tag{2.13}$$

Both sets of equations in conservative or non-conservative form can be extended to an arbitrary fluid volume in order to get their integral form. Of course, for an incompressible flow the density ρ is considered constant, and it can no more be part of the derivatives.

2.1.3 The energy equation

The last governing equation states the physical principle that energy is conserved (first law of thermodynamics). If a fluid element is considered, the equation says the rate of change of energy inside the fluid element is equal to net flux of heat into the element plus the rate of work done on the element by body and surface forces. It's differential conservative form is:

$$\frac{\partial E}{\partial t} + \nabla \cdot (E\mathbf{V}) = \rho\dot{\varepsilon} - \nabla \cdot \dot{\mathbf{q}} - \nabla \cdot (p\mathbf{V}) + \nabla \cdot (\bar{\tau} \cdot \mathbf{V}) + \rho\mathbf{f} \cdot \mathbf{V} \tag{2.14}$$

where E is the total energy per unit volume, function of the internal energy per unit mass e and the kinetic energy per unit mass:

$$E = \rho\left(e + \frac{1}{2}|\mathbf{V}|^2\right) \tag{2.15}$$

Then ε is the volumetric heat (such as radiative heat, for example) absorbed by the control volume per unit time and unit mass, while the heat flux caused by thermal conduction is represented by the term $\dot{\mathbf{q}}$, that is linked to the temperature gradients trough the Fourier's law ($\dot{q} = -k\nabla T$, where k is the thermal conductivity). $\bar{\tau}$ is the viscous stress tensor.
As far as the *non-conservative* differential form of the energy equation is concerned, it is the following:

$$\frac{D}{Dt}\left(e + \frac{1}{2}|\mathbf{V}|^2\right) = \rho\dot{\varepsilon} - \nabla \cdot \dot{\mathbf{q}} - \nabla \cdot (p\mathbf{V}) + \nabla \cdot (\bar{\tau} \cdot \mathbf{V}) + \rho\mathbf{f} \cdot \mathbf{V} \tag{2.16}$$

As for the other governing equations, both 2.14 and 2.16 can be extended over a bigger volume in order to write their integral formulation.

The governing equations are five, but they have to be solved for seven variables, that are ρ, u, v, w, p, e and T. Therefore it possible to model the gas as a perfect gas so that the equation of state and the caloric equation of state can be added to close the system:

$$p = \rho RT \tag{2.17}$$

$$e = c_v T \tag{2.18}$$

where R is the specific gas constant and c_v is the specific heat at constant volume.

From now on, an incompressible flow is considered. This means that the density ρ is assumed constant. As a consequence of that, continuity and momentum equations can be solved separately and can solve the solve the fol field in terms of u, v, w and p. So, since temperature and heat fluxes are non part of the subject of this thesis, the energy equation (as well equations 2.17 and 2.18) can avoid to be solved.

2.2 Numerical simulations: different approaches

In this section different ways of using the governing equations are compared. In particular, different approaches to the problem of modelling turbulent motions are reported. Some of them will be used in the simulations of the next chapters.

2.2.1 Direct Numerical Simulations (DNS)

Given the equations written in the previous section, one way to solve them is to apply them directly to the domain. This approach is called *Direct Numerical Simulation* (or DNS), and its accuracy depends only on the space discretization chosen. Applying this strategy means that all the scales of motion have to be resolved, i.e., according to the Kolmogorov hypothesis, grid spacing must allow the solution for motions in the dissipation range too. As well described by Pope [2], the dissipation range is that range of eddy dimensions whose associated Reynolds number is similar to 1. The smallest of these lengths is known as the Kolmogorov scale. Here, at the bottom of the energy cascade, the molecular viscosity dissipates the kinetic energy coming from the larger scales. So, a grid capable of taking these effects into account has to be very fine and, if applied to the whole domain around the car (this part will be discussed better in the next section), it would account for a huge number of cells. Despite the number of CPUs available, the number of cells obtained would anyway lead to unacceptable computational times. Moreover, with the current computational resources, DNS simulations work well only on simple geometries at low or moderate Reynolds number. For this reason DNS simulations are not employed in common engineering procedures. In order to shorten computational costs, some assumptions are made about turbulence, giving birth to other types of simulation: LES, RANS and DES.

2.2.2 Large Eddy Simulations (LES)

Large Eddy Simulations (LES) are based on the assumption that, as stated by Houghton et al. ([3]), the behaviour of small-scale turbulence is much more universal compared to larger-scale turbulence. So, in this kind of simulations the contributions of the larger-scale motions are resolved, while the small-scale contributions are given by a model. Hence, a spacial filter is imposed: those eddies whose size is greater than the filter are resolved while the smaller ones are modeled. As a consequence of that, the generic velocity component u_i can be seen as:

$$u_i(\vec{x},t) = \tilde{u_i}(\vec{x},t) + u'_i(\vec{x},t) \tag{2.19}$$

In equation 2.19 the term $\tilde{u_i}$ is the resolved component (the filtered one) while u'_i is called the SGS (subgrid-scale) component and $\vec{x}$ is the general osition in space. A filtering operation is applied on the velocity field in order to obtain the filtered velocity in every point of the domain. It is based on the dimension Δ, called filter width. The operation consists of taking an average on a region whose size is Δ, in this way the scales that are smaller than the filter with are removed. It is then possible to apply the filtering operation to the continuity and the momentum conservation equations. Without reporting here all the mathematical formulation (which can be found in [2]), when this operation is done the convective term of the momentum equation gives birth to *residual-stress tensor* $\tau_{r|ij}$.

$$\tau_{r|ij} = \rho\widehat{u_i u_j} \tag{2.20}$$

It is originated by the fact that the filtered product of the velocities is different from the product of the filtered velocities. This term implies a lack of closure of the equation. The most common model used to determine the residual-stress tensor is the Smagorinsky model. According to it, the residual stress-tensor is a function of both the filtered rate rate of strain tensor $\hat{S_{ij}}$ and the Smagorinsky length scale, that can be seen as the product $C_s\Delta$, where C_s is the called the Smagorinsky coefficient. More in details:

$$\hat{S_{ij}} = \frac{1}{2}\left(\frac{\partial \hat{U}_i}{\partial x_j} + \frac{\partial \hat{U}_j}{\partial x_i}\right) \tag{2.21}$$

$$\tau_{r|ij} = -2(C_s\Delta)^2 \hat{S_{ij}} \cdot \hat{S_{ij}} \tag{2.22}$$

The usual practice is to generate an adequate grid and then to set the filter width proportional to the local grid size. This means, then, that the grid (and so the filter) is everywhere fine enough in order to resolve the energy-containing motions.

LES simulations have a cheaper computational cost that DNS simulations and the result is still accurate enough, given that only the small scales require modeling. The assumption of the universal behaviour of the smallest scales requires then that they are independent from the boundary conditions. Accuracy of LES simulations can be increased simply refining the grid, but generally this kind of simulations are still very expensive in terms of computational time and resources in common engineering applications: according to Pope [2], compared to RANS simulations (see next subsection), Large Eddy Simulations are more expensive by approximately two orders of magnitude for each direction of statistical homogeneity.

2.2.3 Reynolds Averaged Navier-Stokes (RANS)

The most common approach in CFD simulations is to use the *Reynolds Averaged Navier-Stokes* equations, or RANS. They are based on the Reynolds decomposition, i.e. instant values of both pressure and velocity are seen as the sum of a mean component and a fluctuating one. Using Einstein's notation:

$$u_i = U_i + u'_i \tag{2.23}$$

$$p = P + p' \tag{2.24}$$

Of course the time mean value of the fluctuating terms is zero, while U_i and P_i are time-independent values. Doing a substitution of equations 2.23 and 2.24 in the governing equations and deleting the negligible terms, if the flow is assumed to have a constant density, the continuity equation and momentum conservation equations become (in Einstein's notation):

$$\frac{\partial U_i}{\partial x_i} = 0 \tag{2.25}$$

$$\frac{\partial U_i}{\partial t} + U_j \frac{\partial U_i}{\partial x_j} = -\frac{1}{\rho}\frac{\partial P}{\partial x_i} + \nu \frac{\partial^2 U_i}{\partial x_j \partial x_j} - \frac{\partial \overline{u_i' u_j'}}{\partial x_j} \tag{2.26}$$

Equation 2.26 is also known as the Reynolds equation and its last term arises from applying the Reynolds decomposition to the velocity components of the Navier-Stokes equations. The term $\rho\overline{u_i' u_j'}$ is called Reynolds stress tensor and accounts for mean flux of momentum due to turbulent fluctuations. It is an other unknown term and has to be determined by a turbulence model in order to close the problem. There are two main models that have this target:

- the *turbulent viscosity hypothesis*
- the *modelled Reynolds-stress transport equations*

The former is the most widely used and is the one used in this work (it will be explained better in the following paragraphs), while the latter relies on a closure model for exact transport equations of the Reynolds stresses, but it less used in common engineering applications and FCA's common procedures do not take it into account.

The turbulent viscosity hypothesis (or Boussinesq's assumption) states that the Reynolds stress tensor $\rho\overline{u_i' u_j'}$ is proportional to the mean strain rate tensor $\overline{S_{ij}}$, defined as:

$$\overline{S_{ij}} = \frac{1}{2}\left(\frac{\partial U_i}{\partial x_j} + \frac{\partial U_j}{\partial x_i}\right) \tag{2.27}$$

In particular, the proportion is given by a term called *turbulent viscosity* or *eddy viscosity* ν_T. In other words, the momentum transfer caused by turbulent eddies can by modelled with an eddy viscosity. More in details:

$$-\rho\overline{u_i' u_j'} + \frac{2}{3}\rho k \delta_{ij} = 2\rho\nu_T \overline{S_{ij}} = \rho\nu_T\left(\frac{\partial U_i}{\partial x_j} + \frac{\partial U_j}{\partial x_i}\right) \tag{2.28}$$

where k is the mean turbulent kinetic energy per unit mass, which is a function of the Reynolds stresses.

$$k = \frac{\overline{u_i' u_j'}}{2} \tag{2.29}$$

Now, the new unknown is the eddy viscosity. It is responsible for how much the turbulence affects the mean flow. The operation of expressing this term is called *turbulence modelling*, and there are several ways to do it. Some of them express the eddy viscosity ν_T as a function of a dimension called *mixing length*, that as to be specified according to the geometry of the flow. The most popular model in industrial application, tough, is the k-ϵ model, that is implemented in the software STAR-CCM+. It is chosen to use it in most of this work and the next subsection shows how it works. Its main rival is the k-ω model, and its formulation is reported after the k-ϵ model.

The k-ϵ model

The k-ϵ model gives a solution for the eddy viscosity without taking into account the mixing length. The turbulent viscosity is written as a function of the turbulent kinetic energy k (previously defined in equation 2.29) and the turbulent dissipation ϵ:

$$\nu_T = C_\mu \frac{k^2}{\epsilon} \tag{2.30}$$

where C_μ is one of the coefficients used by this model. So both k and ϵ have to be determined. To do that two equations are needed. The firs one is the transport equations for the turbulent kinetic energy k. It is obtained with some manipulations of the Navier-Stokes equations and the Reynolds equations. It is the following:

$$\frac{\partial k}{\partial t} + U_i \frac{\partial k}{\partial x_i} = \Pi - \epsilon - \frac{\partial I_i}{\partial x_i} \tag{2.31}$$

where Π is called the production term, and contains the turbulent energy given by the interaction between the mean flow and the turbulence. It is defined as:

$$\Pi = -\overline{u_i' u_j'} \frac{\partial U_i}{\partial x_j} \tag{2.32}$$

In equation 2.31,then, I_i is the diffusion term, expressed as:

$$I_i = -\frac{\nu_T}{\sigma_k} \frac{\partial k}{\partial x_i} \tag{2.33}$$

where σ_k is a model constant. As far as the equation for the turbulent dissipation rate is concerned, an entirely empirical one is applied. Given that the exact equation for the turbulent dissipation rate ϵ refers to the dissipative range (at the bottom of the energy cascade), this artificial equation sees ϵ as the energy flow rate that starts from the large-scale motions (where its value is determined) and is transferred towards the small-scales. It is the following:

$$\frac{\partial \epsilon}{\partial t} + U_i \frac{\partial \epsilon}{\partial x_i} = C_{\epsilon 1} \frac{\epsilon}{k} \Pi - C_{\epsilon 2} \frac{\epsilon^2}{k} + \frac{\partial}{\partial x_i} \left(\frac{\nu_T}{\sigma_\epsilon} \frac{\partial \epsilon}{\partial x_i} \right) \tag{2.34}$$

Several coefficients are used by the k-ϵ model. Their values were determined empirically. They are:

$$C_\mu = 0.09 \quad C_{\epsilon 1} = 1.44 \quad C_{\epsilon 2} = 1.92 \quad \sigma_k = 1.0 \quad \sigma_\epsilon = 1.3 \tag{2.35}$$

So, when a flow field has to be resolved and it is chosen to use the k-ϵ model, also equations 2.31 and 2.34 are discretized and solved. It was shown that the k-ϵ model is very reliable for regions located away from the walls, while it needs some wall functions to manage the boundary layers. It can be inaccurate when separation occurs or when an adverse pressure gradient is present. Anyway its computational cost is quite inexpensive compared to other models.

The k-ω model

An other important two-equation turbulence model is the k-ω model. As well described by Wilcox [4], it shows a different way to calculate the turbulent viscosity ν_T (or eddy viscosity). This time it can be expressed as:

$$\nu_T = \frac{\rho k}{\overline{\omega}} \tag{2.36}$$

with:

$$\overline{\omega} = \max\left[\omega, C_{lim}\sqrt{\frac{2\bar{S}_{ij}\bar{S}_{ij}}{\beta^*}}\right] \tag{2.37}$$

$$C_{lim} = \frac{7}{8} \tag{2.38}$$

In the previous equations k is again the turbulent kinetic energy and $\overline{\omega}$ is the effective specific dissipation rate that is used to compute the eddy viscosity. It can be equal to ω, that is the specific dissipation rate, or it can be a function of the stress limiter coefficient C_lim and of the averaged strain-rate tensor $\overline{S_{ij}}$. β^* is one of the model closure coefficients. The parameters k and ω are governed again by two equations:

$$\frac{\partial}{\partial t}(\rho k) + \frac{\partial}{\partial x_j}(\rho u_j k) = \rho\overline{u_i u_j}\frac{partialu_i}{\partial x_j} - \beta^*\rho k\omega + \frac{\partial}{\partial x_j}\left[\left(\mu + \sigma^*\frac{\rho k}{\omega}\right)\frac{\partial k}{\partial x_j}\right] \tag{2.39}$$

$$\frac{\partial}{\partial t}(\rho\omega) + \frac{\partial}{\partial x_j}(\rho u_j\omega) = \rho\overline{u_i u_j}\alpha\frac{\omega}{k}\frac{\partial u_i}{\partial x_j} - \beta\rho\omega^2 + \sigma_d\frac{\rho}{\omega}\frac{\partial k}{\partial x_j}\frac{\partial\omega}{\partial x_j} + \frac{\partial}{\partial x_j}\left[\left(\mu + \sigma\frac{\rho k}{\omega}\right)\frac{\partial\omega}{\partial x_j}\right] \tag{2.40}$$

All the coefficients that appear in the previous equations (σ^*, β^*, α, β, σ_d, σ) are closure coefficients. Their values, reported by Wilcox [4], are obtained empirically.

The k-ϵ model is the most popular one in the automotive industry for steady-state external aerodynamic simulations, since its main advantages are given by its stability and its quick convergence rate. As a drawback, the k-ϵ model is inaccurate in presence of separation, adverse pressure gradients or swirling and rotating flows. Moreover, it needs wall functions to resolve the flow field in near wall areas. On the contrary, the k-ω model performs significantly better under adverse pressure gradients conditions, even tough it generally requires a higher mesh resolution near the wall.

As described in the previous lines, the solutions obtained from RANS equations gives the averaged flow field. Hence it reasonable to apply them for steady-state simulations. Unsteady RANS equations (or URANS) can be used as well, but in this case the meaning of averaging changes, and the average flow field for every time-step is found.

2.2.4 Detached Eddy Simulations (DES)

The last approach to the governing equations that is briefly described is the *Detached Eddy Simulations*. It is the most recent one and in the last years its implementation in the procedures for the common industrial application has risen quite sensibly. This method aims to combine the most favourable aspects of both RANS and LES simulations. In particular RANS technique is used to predict the attached boundary layer, while the LES technique is used to solve the large eddies. In facts, DES turbulence models are set up so that boundary layers and irrotational flow regions are solved using a base RANS closure model while it will emulate a basic LES sub-grid scale model in detached flow regions. In this way, it is possible to get the best of both worlds: a RANS simulation in the boundary layers and an LES simulation in the unsteady separated regions.

2.3 Spacial discretization and time integration

A method to solve the equations that govern the fluid phase and the turbulence modelling is described in this section. Since an analytical solution to the governing equations of fluid dynamics still has to be found, a numerical procedure has to be applied in order to find an approximate solution to the problem. Commercial CFD codes such as STAR-CCM+ rely on the integral form of the equations, that has the same meaning of the differential ones, except for the fact that now the equations are applied on the entire fluid domain. In order to solve the governing equations and get a solution for every point of the domain, the *finite volume* discretization is used. According to this method, the fluid domain is divided in smaller volumes, or cells, and a computational node is assigned to the center of each cell. The boundary conditions are then assigned to the boundary surfaces of the computational domain. The governing equations hold for each cell, but also for the computational domain as a whole. If all the equations written for every cell of the domain are summed, the global conservation equation is obtained. The operation of dividing the domain in cells is called *mesh generation* and this topic will be well described in the next section. An important property of the mesh generation is called *consistency*: a numerical solution is said to be consistent if it tends to the exact solution when the grid spacing tends to zero (see what said about the DNS in section 2.2.1).

Once the domain has been discretized, the governing equations in their integral form are applied to each cell. It is important to point out that, as mentioned in the previous sections, for all the simulations run for this thesis density is assumed constant. When this assumption is made, continuity equation and momentum conservation equation are sufficient to solve the flow field. This means that the energy equation is not needed anymore, given that the unknowns to be found are p, u, v and w. A smart way to resolve this system of equations for a steady-state case is given by the SIMPLE (Semi-Implicit Method for Pressure Linked Equations) algorithm, that is implemented in STAR-CCM+. This algorithm is based on the pressure correction procedure. More in details, given an initial solution at the iteration k, it can be described by the following steps:

- the pressure at iteration k is used to find the velocity components from the momentum conservation equations: these components are now called $u*$, $v*$ and $w*$.
- the continuity equation 2.3 has to be satisfied with the velocity components just found. As written at the previous point, the value p^k leads to the velocities $u*$, $v*$ and $w*$. They do not necessarily satisfy the continuity equation, though. Hence, using the continuity equation a pressure correction p' is obtained such that, when added to p^k it will give a pressure that is more into agreement with the continuity equation.

  $$p^{k+1} = p^k + p' \tag{2.41}$$

  The velocity corrections u', v' and w' can be obtained from the pressure correction p' though the momentum conservation equations, so that:

  $$u^{k+1} = u^k + u' \tag{2.42}$$

  $$v^{k+1} = v^k + v' \tag{2.43}$$

  $$w^{k+1} = w^k + w' \tag{2.44}$$

- The process can start again with a new iteration until a velocity that satisfy the continuity equation is found.

This algorithm allows to determine the flow field for a steady-state simulation.

As far as transient simulation are concerned, two methods are available: the explicit method and the implicit method. The first one exploits the the solution at the previous time-step in order to calculate the new solution. Hence Δt needs to be very in small, given that the the CFL (Courant-Friedrichs-Lewy) condition has to be satisfied, i.e. the a fluid particle must not travel for more the a cell length per time-step. This means that the Courant number has to be lower than unity:

$$\frac{u_i \Delta t}{\Delta x_i} < 1 \tag{2.45}$$

On the other hand, an implicit method allows larger values for Δt, since it uses a different approach: the iterations are divided between internal and external ones. External iterations deal with time, and they take into account the time derivatives terms of the governing equations, while the internal ones are used to reach convergence at every time-step, considering the stationary part of the governing equations.

2.4 CFD domain and mesh

As mentioned before, numerical techniques used to solve the flow field need the domain to be divided in finite volume elements, or cells, in witch the equations sill hold. So the first things that have to be determined when setting up a simulation are the fluid domain and its discretization, or mesh. The next subsections will deal with the domain choice and then the mesh generation.

2.4.1 Fluid domain

As far as fluid domain is concerned, working with the flow field around a vehicle, two choices are possible: the first one is to use an ”open air” domain, while the second one is to use the ”wind tunnel” domain. Both are made by the geometry of the vehicle and a plane under its wheel in order to simulate the road surface. If this plane is seen as one face of a parallelepiped whose longitudinal dimension is aligned with the longitudinal dimension of the car (from now on the x axis), then the position of the other faces needs to be determined. This position is the difference between the two domains.

- The ”open air” domain is a box whose walls are very far from from the vehicle and they do not affect neither the aerodynamic field near the vehicle nor the forces acting on it. The inlet and the outlet of the domain then are far upstream and very far downstream with respect to the position of the vehicle, so that the wake can fully develop within the domain. This is the standard domain used at FCA for the external aerodynamics simulations.
- On the other hand, the ”wind tunnel” domain is a smaller box, whose walls are much closer to the car. In particular its section is exactly the same as that of FCA Climatic Wind Tunnel located in Orbassano, that is, as mentioned in the Introduction, the facility where water ingestion test (or *Slipstream test*) takes place. Given that the results of CFD simulations will be compared to those coming from this test and to a water soiling test too, it is chosen to use this kind of domain, being closer to the experimental conditions. Exactly in the same way as it happens in the wind tunnel, there will be a blockage effect in the numerical solution, caused by the proximity of the walls to the car. Therefore it will be meaningless to measure quantities such as forces and their coefficients when this domain is being used. This domain is shown in Figure 4.1.

2.4.2 Mesh

As far as mesh is concerned, it is affected by many issues. First of all, the domain discretization must be quick to generate and has to be a good compromise between the calculation speed (i.e. convergence rate) and a good level of accuracy. The accuracy level is usually said to be good when the results match the experimental ones (coming from the wind tunnel, for example) or when a convergence analysis is made. A convergence analysis consists of running the same simulation several times with different mesh sizes. Convergence is reached when, refining the mesh at each step, the results do not change. The coarsest grid still capable of giving those results has to be chosen as the standard mesh to use for those kind of simulations. So, it is a compromise between the computational costs (a finer mesh always requires more resources) and the desired accuracy. The correlation with the experimental results then gives the possibility to understand whether the results obtained are finally reliable or not. What just described is a general approach to the problem of finding the right volume discretization, and can be applied to the C_d investigation of a road car. FCA has its own parameters to use in a case such as external aerodynamics and they are very reliable when it gets to estimate the drag of the vehicle in an open air domain, for example. Now the purpose of this thesis is to investigate vehicle soiling and engine water ingestion. These two phenomena are not part of the standard procedures of the company, so a specific set of grid parameters for these simulations is not present. Despite the fact that there are few experimental data to use as comparison (specially for the soiling simulations), to perform a convergence analysis would require too much time. As a consequence of that the grid used for external aerodynamics is assumed to be good enough for these multiphase simulations.

To generate a mesh that is capable to give an accurate result means to have a general understanding of what actually happens in the flow field. Indeed a wider cell size can be used where the flow is almost uniform, such as at the beginning of the domain (just after its inlet). On the other hand finer cells are needed where strictly three-dimensional turbulent structures are expected, such as in the wake of the vehicle. Moreover, attention must be paid to the boundary layer discretization. On many boundaries of the domain that will be simulated, a no-slip condition is assumed, i.e. $V = 0$ at the wall. It means that a boundary layer has to be solved on that boundary. To do that, the space that is closer to the wall is discretized in several *prism layers* (they are thin prismatic cells) in order to better catch the velocity gradients in the normal direction with respect to the wall. The volume discretization that takes place beyond the last of these layers is usually called the *core mesh*.

As far as the prism layer mesh is concerned, it is very important to generate it properly if the target of the simulation is to determine the vehicle drag coefficient C_x. These cells have to catch the velocity gradients in order to describe the boundary layer velocity profile. What's more, they are responsible for the determination of the separation point, that is critical for the drag determination, being the point beyond which the pressure drops. The first cell centroid distance from the wall is used to calculate the wall non-dimensional distance y^+. This is defined as:

$$y^+ = \frac{y u_\tau}{\nu} \tag{2.46}$$

where u_τ is the friction velocity, and y is the distance from the wall. The friction velocity is defined as:

$$u_\tau = \sqrt{\frac{\tau_w}{\rho}} \tag{2.47}$$

The y^+ has to be correlated with the wall non-dimensional velocity u^+:

$$u^+ = \frac{u}{u_\tau} \tag{2.48}$$

In particular, the correlation between u^+ and y^+ is expressed by the *law of the wall.* This empirical law is used to model what happens within the inner layer of the boundary layer. In particular, the following relation is assumed:

$$u^+ = \begin{cases} y^+ & \text{if } y^+ < 5 : \text{ viscous subllayer} \\ \frac{1}{k}\log y^+ + c & \text{if } y^+ > 50 : \text{ log region} \end{cases} \tag{2.49}$$

Where $k = 0.41$ and $c = 5$. The law states that the velocity profile in the viscous sublayer ($y^+ < 5$) is linear: here the viscous stresses are dominant. The relation becomes logarithmic in the log region (i.e. $y^+ > 50$), where the shear stresses prevail. The range of wall distance $5 < y^+ < 30$ is where the buffer layer is located. Here there shear and viscous stresses are comparable with each other. So, when it comes to generate the mesh it is important to have an idea of what value of y^+ will be obtained on each wall. In particular the thickness of the first prism layer sets the value of y^+ wanted. A small value makes the simulation capable of catching the viscous sub-layer while a larger one makes the first centroid to be in the logarithmic region. When this happens some "wall functions" are implemented in STAR-CCM+ in order to take into account the effects of the viscous sub-layer, even tough it is not directly detected. It is a good practise not to fall in the buffer layer, since it is a transitional region and the solution can be less accurate.

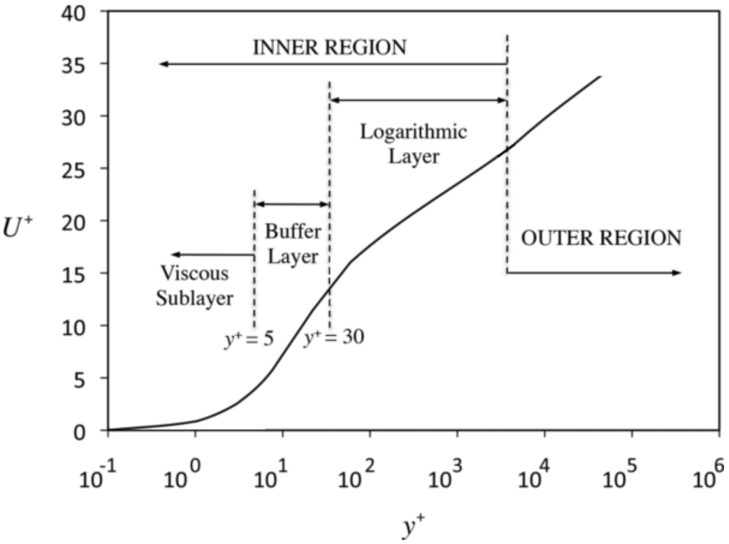

Figure 2.1: The law of the wall

An important choice is the type of elements chosen for the core mesh: two main choices can be made in STAR-CCM+:

- *polyhedral cells*: if the number of cells is fixed, they provide the highest level of accuracy, but it takes much more time to generate them, as only one processor can be used. Hence, their main drawback is the serial mesh generation.

- *trimmed cells*: they are prism cells that make a structured grid. An adequate number of trimmed cells can of course reach the same accuracy of a smaller number of polyhedral cells. The advantage of using trimmed cells is the parallel use of several processors to generate them, resulting in less time spent for meshing.

As far as simulations that will be executed are regarded, common FCA internal procedures are used. In particular trimmed cells are used for the core mesh. They have several refinement boxes in witch their size is reduced in order to have a more accurate solution in those areas. These boxes are located around and behind the wheels of the vehicle, around its hood intakes, A and C pillars, rear view mirrors, dam, locaries and spoiler. What's more, several boxes are located around the whole car and its wake and some of them extend until the domain outlet. Using this kind of setting, the mesh accounts for about 90 millions cells.

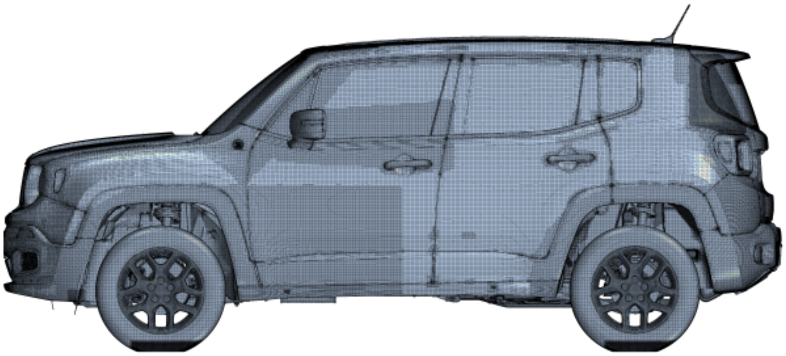

Figure 2.2: Mesh on the surface of the vehicle, refinement volumes are visible on A and C pillars of the vehicle, on the rear view mirror and on the wheels

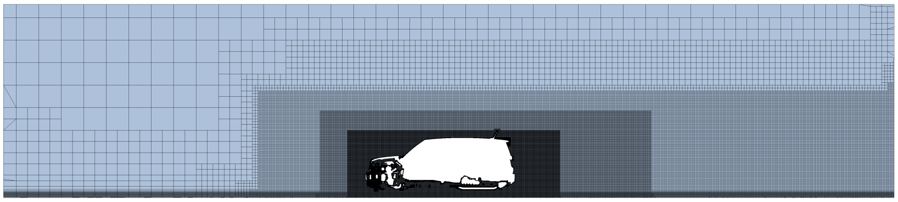

Figure 2.3: Mesh on the x-z plane of the domain, all the wake refinement boxes are visible

2.5 Porous media

In order to complete all of the aspects concerning a vehicle CFD simulation, porous media modeling is now introduced. In fact, several of them can be be found on board. In particular, in the case of Jeep Renegade, they are radiator, inter-cooler, and condenser. Moreover, for water ingestion simulations, the engine intake filter is considered a porous medium as well. A porous medium is a structure made of solid elements permeated by fine-scale voids that can allow the passage of a fluid such as air (see [5]). To include all of this complex geometry in the simulation is difficult because it would require a very a very fine mesh in order to catch all the phenomena inside them. Hence, a quicker way to take their effect into account is exploited. These volumes are represented simply as blocks, whose geometry is defined by an inlet, an outlet, and four walls. From a porous medium, such as a radiator, its pressure/velocity curve can be obtained empirically, where the velocity considered is the one normal to the inlet of the block. Interpolating the curve with a parabola, the following relation can be obtained:

$$-\frac{\Delta p}{L} = P_v U_n + P_i U_n^2 \tag{2.50}$$

where U_n is the velocity mentioned before, L is the thickness of the block (in the same direction as the fluid is moving) and P_v and P_i are two coefficients, called respectively *porous viscous resistance* and *porous inertial resistance*. These two terms have to be specified within STAR-CCM+. So, using this model, what happens inside the porous medium is not simulated, but its effect is reflected on the flow that crosses it.

Chapter 3

Multiphase models

Now that a brief description of how a generic incompressible flow is modeled and solved, the problem of dealing with dispersed water in it has now to be faced. This Chapter deals with numerical models developed with this purpose. In particular the first section focuses on the physics of the problem to be modeled (i.e. the exterior water management of a vehicle), then the second section is about the Dispersed Multiphase model (or DMP), that treats water from an Eulerian point of view. Section 3.3, then, deals with the Lagrangian Multiphase model, and it is finally followed by the Fluid Film model and its sub-models.

3.1 Multiphase flows: main features

A multiphase flow is a flow that comprehends two or more phases. In a different manner from the common definition of phase used in chemistry (i.e. the thermodynamic state of matter: solid, liquid or gas), here a phase is defined as a certain amount of matter having its own physical properties and behaviour. According to this definition, different phases within the same system can be, for example, two liquids with different densities, dispersed bubbles with different size or even dispersed particles with different sizes. As far as the flow around a vehicle is concerned, rain droplets can be considered as a phase, and droplets of another size can be considered a different phase.

As well described by Hagemeier et al. [6], a vehicle advancing on a road in rain conditions is subject to water contamination by three main sources. They are:

- wind driven rain: it is the most important of the three sources and its contribution is affected by the speed of the vehicle in terms of both the relative velocity of the water droplets and their angle of attack.
- liquid raised by other vehicles: this can be relevant in particular when the other vehicle is a heavy one, such as a bus or a lorry, whose wake has a big size and can entrain (and then lift) a lot of droplets coming from its own wheels. The intensity of this source is usually one order of magnitude lower than the wind driven rain.
- self-soiling due to the rotation of the wheels of the car: tyres can in fact lift some water from the ground and spread it on the side of the vehicle. Like in the previous case, the intensity of the source is one order of magnitude lower than the wind driven rain. This effect is the most difficult one to take into account in numerical simulations.

Once a droplet gets closer to the car, it is important to define its behaviour. First of all, depending on its size and mass, that are related to the source the droplet is coming from, the motion of the particle will be more or less affected by the surrounding flow field. In other words, if the inertial forces of the droplet prevail on the aerodynamic ones, then its path will be different from the one given by the air streamlines. On the contrary, a droplet will follow the streamlines if it is dominated by the aerodynamic forces. The Stokes number is a good index of how much the particles are affected by the surrounding fluid. It is defined as:

$$Stk = \frac{t_0 V}{D} \tag{3.1}$$

where V is the surrounding fluid velocity, D is the characteristic dimension of an obstacle that obstructs the flow and t_0 is the particle response time (or relaxation time), i.e. the time needed by the particle to respond to a change of the velocity of the fluid and to follow this new velocity so that in can move around the obstacle. A Stokes number much greater than unity usually means that the particle is unaffected by air (that is, inertial forces prevail), while it perfectly follows the streamlines if its Stokes number is lower than unity. The response time can be expressed as:

$$t_0 = \frac{d^2 \rho_d}{18\mu} \tag{3.2}$$

where ρ_d is the particle density, d is its diameter and μ is the surrounding air dynamic viscosity. The Stokes number then becomes:

$$Stk = \frac{\rho_d d^2 V}{18\mu D} \tag{3.3}$$

It is now possible to estimate the Stokes number of a rain droplet. Assuming the droplet diameter as $d = 0.001m$, its density $\rho_d = 1000kg/m^3$, the air density $\mu = 1.81\ 10^{-5} Pas$, the air velocity $V = 22.22m/s$ (80km/h), and $D = 2m$ as a characteristic dimension for a vehicle, the resultant Stokes number is $Stk = 34$, that is greater than 1. This means rain droplets at 80km/h do not follow the air streamlines around the car, but have their own trajectories and, as one can see travelling in a rainy day, they contact the car.

The phenomenon of a droplet contacting a surface is called *impingement*. When it happens, water that remains on the surface is then part of a *fluid film*. During the impingement, a droplet can bounce back (its mass is still dispersed in the air after the impingement), stick (its mass becomes part of a fluid film on the surface) or break up (the mass partially stick and bounces back). This means that, from case to case, mass, momentum and energy of the droplet can be fully or partially transmitted to the fluid film that is starting to grow on the surface.

As far as fluid film is concerned, it starts growing where the first droplets impinge and then it moves on the surface as a true film or as water rivulets. It is driven by the shear stress done by the air stream on the water surface and by the gravitational force. It is then possible to see a certain amount of water leaving the film: this phenomenon is called *stripping* and it can happen in two ways. The first one is the wave stripping. Given a fluid film on a plain surface, it happens when the small waves formed on the film-air interface reach an instability and some droplets detach and get entrained by air stream. The second one is the edge stripping and it occurs when the water film meets a sharp edge. Here droplets are generated from the film and are taken away by the air stream. In this situation the inertial forces of the water make it leave the surface. Of course a *re-impingement* is possible: it happens when a droplet leaves a fluid film and then reaches an other surfaces, so that the process can start again.

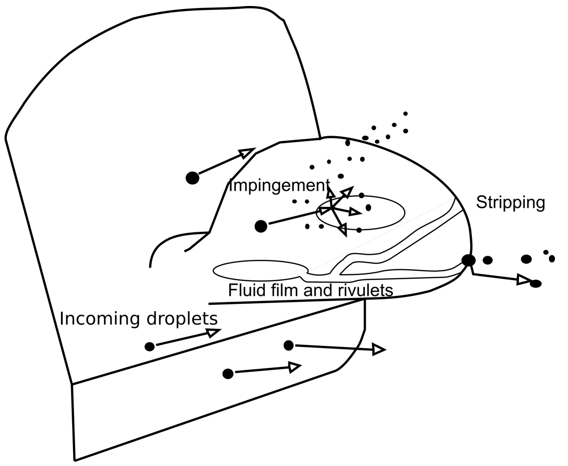

Figure 3.1: Scheme of the water behaviour on a generic rear view mirror of a car

3.2 Dispersed Multiphase model (DMP)

The first multiphase model used is called *Dispersed Multiphase* model, or DMP. This model is part of the software STAR-CCM+ (see [5]) and has to be used when small particles are carried by a continuum stream around the domain. It fits very well for soiling investigation, given that the rain droplets are brought towards the vehicle by the relative wind. In particular, the DMP solves continuity and momentum equations in terms of volume fraction and velocity of the dispersed phase. Therefore this is an Eulerian point of view. It is important to distinguish the dispersed phase, such as rain water in this study, from the background flow, that is the air flow around the vehicle. In particular this model imposes a one-way coupling, i.e. the background flow can influence the dispersed phase (with drag force, for example), but the opposite is not allowed. This fact is also known as *interpenetrating continua*. The equations solved by this model are the following:

$$\frac{\partial}{\partial t}(\alpha_d \rho_d) + \nabla \cdot (\alpha_d \rho_d V_d) = 0 \tag{3.4}$$

$$\frac{\partial}{\partial t}(\alpha_d \rho_d u_d) + \nabla \cdot (\alpha_d \rho_d u_d V_d) = S_x \tag{3.5}$$

$$\frac{\partial}{\partial t}(\alpha_d \rho_d v_d) + \nabla \cdot (\alpha_d \rho_d v_d V_d) = S_y \tag{3.6}$$

$$\frac{\partial}{\partial t}(\alpha_d \rho_d w_d) + \nabla \cdot (\alpha_d \rho_d w_d V_d) = S_z \tag{3.7}$$

Equation 3.4 is the continuity equation for the dispersed flow, where α_d is its volume fraction ($0 < \alpha < 1$). The subscript d stands for "dispersed phase". As it can be understood by its formulation, this model treats the water droplets as a continuum, even tough they are not. It does not track each particle, but gives a value of volume fraction and velocity in every point of the domain. Therefore α_d can be seen as the probability of finding the dispersed phase in that point at that time. The right hand side of equation 3.4 is non-zero if in that point there is source of dispersed phase, such as fluid film stripping or the domain inlet.

Momentum conservation for the dispersed phase is expressed by equations 3.5, 3.6 and 3.7, that are solved for the dispersed phase velocity components u_d, v_d. w_d. The generic term S_i that appears on the right hand side of those equations takes into account several effects linked to the dispersed phase. In the case of vehicle soiling S_i is made by the contributions of the gravity force per unit volume ($\alpha_d \rho_d g$), by the pressure gradients ($\alpha_d \frac{\partial p}{\partial x_i}$) and by the drag force acting on the particles. To estimate this drag force, a sphere is firstly considered: if this sphere is assumed to be a dispersed particle whose diameter is d, then its volume can be expressed as:

$$V_{sphere} = \frac{\pi d^3}{6} \tag{3.8}$$

Moreover one can get its interface area A_s, that is the surface area of the sphere, and its projected area A_p, or its frontal area. They are expressed as:

$$A_s = \pi d^2 \tag{3.9}$$

$$A_p = \pi \frac{d^2}{4} \tag{3.10}$$

Now, since the volume fraction of the dispersed phase is defined as $\alpha_d = \frac{V_d}{V_{tot}}$, if there are n spherical particles, then the volume V_d occupied by them becomes (from equation 3.8):

$$V_d = n \frac{\pi d^3}{6} \tag{3.11}$$

So the number of particles can be obtained:

$$n = \frac{6V_d}{\pi d^3} = \frac{6\alpha_d V_{tot}}{\pi d^3} \tag{3.12}$$

The overall interface area of the dispersed phase therefore is (see equation 3.9)

$$A_{sd} = n\pi d^2 = \frac{6\alpha_d V_{tot}}{d} \tag{3.13}$$

and the interface area per unit of volume is then:

$$A_{sdv} = \frac{6\alpha_d}{d} \tag{3.14}$$

Observing equations 3.9 and 3.10, one can notice that $A_p = \frac{A_s}{4}$. The same relationship holds in a unit of volume, and the drag force acting on the dispersed phase per unit of volume can be written:

$$f_{di} = \frac{1}{2} \rho C_D A_{pdv} {\Delta u_i}^2 = \frac{1}{8} \rho C_D A_{sdv} {\Delta u_i}^2 \tag{3.15}$$

In equation 3.15 ρ is the density of the background phase (air), C_D is the particle drag coefficient, A_{pdv} is the overall frontal area of the dispersed phase per unit of volume and Δu_i is the relative velocity between the dispersed and the background phase (i.e. between water and air). The final expression for the drag force per unit of volume that acts on the dispersed droplets is get putting equation 3.14 into the previous one:

$$f_{di} = \frac{3}{4} \rho C_D \frac{\alpha_d}{d} {\Delta u_i}^2 \tag{3.16}$$

The drag force then, is calculated starting from the volume fraction α_d and the particle diameter d. The drag force is expected to rise when the diameter d is increased, since the droplet frontal area is increased as well. Despite this logical consequence, though, equation 3.16 seems to tell the opposite, since d appears in the denominator. Actually, tough, both the drag coefficient and the volume fraction (that appear in the numerator) are indirectly affected by the diameter d. The volume fraction of the dispersed phase is indirectly affected by the droplet diameter because a bigger droplet simply has a bigger volume. As far as the drag coefficient is concerned, a well established method to get it is to use the *Schiller-Naumann* model. It is based on the particle Reynolds number, defined as follows (here d appears again):

$$Re_d = \frac{\rho d \Delta v}{\mu} \tag{3.17}$$

where both ρ and μ refer to background phase. According to the Schiller-Naumann model, the drag coefficient is assumed as:

$$C_D = \begin{cases} \dfrac{24}{Re_d} & \text{if } Re_d \leq 1 \\ \dfrac{24}{Re_d}\left(1 + 0.15{Re_d}^{0.687}\right) & \text{if } 1 < Re_d < 1000 \\ 0.44 & \text{if } Re_d \geq 1000 \end{cases} \tag{3.18}$$

Now the drag force per unit of volume acting in one point can be determined. Of course it acts in the same direction of the DMP velocity, but with opposite sign. Its components, together with those of the pressure gradient and gravity forces (mentioned before), contribute to the right hand term of equations 3.5, 3.6 and 3.7. As seen from the expression of the drag force, the particle diameter has to be assigned when this model is applied.

3.3 Lagrangian Multiphase model

In this section the Lagrangian Multiphase model will be described. In the same way as the DMP model works, this model solves for the dispersed phase only, i.e. it does not solve for the velocity and pressure fields of the background phase. So, just as it happens for the DMP, the equations of this model have to be resolved together with the governing equations. The purpose of the Lagrangian Multiphase model is to describe the trajectory of each particle in terms of particle position and velocity at every instant. It is not difficult to imagine that for many applications, the number of particles to track can be huge, and therefore the computation of all the trajectories can result very expensive. To overcame this difficulty, the software STAR-CCM+ (see [5]) uses a statistical approach. So, to avoid keeping track of each single single particle, this approach separates the *particle* and the *parcel*. More in details:

- A *particle* is a single droplet, bubble or small solid that is dispersed in a fluid continuum (i.e. the background phase). Every particle has its own dimension.
- A *parcel* is a set of identical particles that have the same properties (for example the same mass, density, velocity, diameter, or volume). Within a parcel , particle do not interact with each other. Different parcels can collimate, coalesce, breakup, bounce off the wall or impinge on it. As a consequence of its definition, the mass of a parcel is the sum of the mass of all particles contained in that parcel.

So, using the statistical-mathematical concept of parcel, it is possible to save a lot of computational time and memory, given that what is tracked is now the parcel. Therefore the solution obtained by the Lagrangian Multiphase model consists of the the trajectories of the mean centroids of the parcels. In the same way, the velocity of the centroid of a parcel is the velocity of all of its particles. So a parcel can be seen as a discretization of the dispersed phase: assuming that all the particles have the same property, they can all be part of the same parcel, but this would result on just one trajectory to be found. In the case of rain, for example, this would be completely unrealistic. It follows that the number of particles per parcel has to be specified (directly or not), in order to have a realistic number of trajectories for the dispersed phase. The correct number is usually found with different tries and doing a trade-off between the final results and the computational time required to get it.

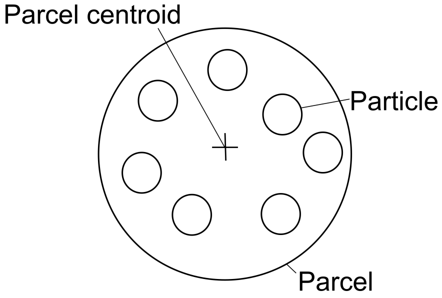

Figure 3.2: Representation of a parcel and its particles. In the example all the particles have the same diameter

As far as the link between the position of the parcel (r_p) and its velocity (v_p), it is given by the following simple equation of motion:

$$\frac{\mathrm{d}r_p}{\mathrm{d}t} = \mathbf{V}_p \tag{3.19}$$

Then, a mass conservation equation has to be written. In the case of rain, there are no evaporation processes or other mass-exchange phenomena, so the mass of the water droplets has to be constant:

$$\frac{\mathrm{d}m_p}{\mathrm{d}t} = 0 \tag{3.20}$$

Equation 3.20 is true everywhere in the flow field except where the sources are located. In facts, it is convenient to specify some points inside the domain that can act as injectors. The injectors are locations where the right hand term of equation 3.20 is non-zero. Here a source of Lagrangian phase is located. As explained in the next section, an injector can also be automatically placed where fluid film stripping is detected.

Now the momentum conservation for a Lagrangian parcel is written. It is the Newton's Law in its simplest form:

$$m_P \frac{\partial \mathbf{V}_p}{\partial t} = \mathbf{F}_b + \mathbf{F}_s \tag{3.21}$$

where $\mathbf{F}_b$ is the sum of all body forces acting on the parcel and $\mathbf{F}_s$ is the sum of the forces acting on the surface of the particles. The surface forces acting on a rain droplet are mainly two (as already told in the previous section): the pressure gradient forces and the drag force. Then, the only body force acting on a rain droplet that travels towards a vehicle is the gravity force. All other forces can be neglected. The drag force can be written as:

$$\mathbf{F}_d = \frac{1}{2}\rho C_D A_p |\mathbf{V}_p| \mathbf{V}_p \tag{3.22}$$

where ρ is the density of the surrounding fluid (air), C_D is the drag coefficient of the particle, that can be obtained with the Schiller-Naumann model (see equation 3.18), A_p is the frontal area of the particle and V_P is the particle velocity in that point. So, in order to know the frontal area, if the particle is assumed to be spherical, a diameter must be assigned. As far as the pressure gradient force is concerned, it is given by:

$$\mathbf{F}_p = -\zeta_P \nabla p \tag{3.23}$$

where ζ_P is the volume of the particle and ∇p is the pressure gradient of the background phase. The last force taken into account is the gravity force, that can be expressed as follows:

$$\mathbf{F}_g = m_P \mathbf{g} \tag{3.24}$$

where $\mathbf{g}$ is the gravity vector.

What described in the previous paragraphs is a quite simple model, but it can be accurate enough to catch the global behaviour of the rain droplets. Actual rain droplets can have much more complex dynamics, in fact, they can be subject to collision (two or more droplets get in contact with each other) or break-up (a droplet can give birth to one or more other droplets). Given that simulating rain involves a high number of parcels to track, it is chosen not to involve models for these two phenomena. To take into account droplet collision and break-up would increase the computational cost and the simulation time and it would consist of very little increase in the accuracy of the results. The Lagrangian Multiphase solver is generally much more expensive than the Dispersed Multiphase model, but it is more accurate. Tracking a particle over its path is much more precise than estimating its volume fraction in the background phase, as the DMP does. As stated in the DMP section, the resulting volume fraction has to be read as a probability of finding a droplet in a particular point, while the Lagrangian Multiphase model is capable of providing the exact position of the droplets. As mentioned, its biggest drawback is its cost: as it will be seen in the following chapters, a Lagrangian simulation can require even more than three times the time needed by the DMP. As a consequence of that, every sub-model (such as break-up, collision and so on) must be cautiously evaluated before applying it. A sub-model implemented in STAR-CCM+ that can help in this cases, is called *parcel depletion*. Basically it uses an arbitrary condition to delete the parcels from the domain. For example an x coordinate in the domain (away from the area of interest) can be set as a limit beyond which all the parcels are deleted. This procedures can save a lot of time and resources.

3.4 Fluid Film Model

In order to study what happens after the collision between a particle and a solid surface, a fluid film model can be activated in STAR-CCM+. The purpose of this model is to avoid the creation and the simulation of a specific domain just for the water. In other terms, the fluid film acts as a two-dimensional model and the discretization used is determined by the faces of the near-wall cells that lie on the boundary. In this way a specific volume of fluid with its own cells can avoid to be created. This would require a much finer grid on the boundary where the water layer is expected to grow and then, in these cells, the governing equations for the water phase would have to be solved. By using the fluid film model a lot of time is saved: no mesh is required and can be applied only to the surfaces of interest.

The fluid film model used by STAR-CCM+ is based on some assumptions (see [5]):

- the film is thin enough, so that laminar boundary layer is assumed. If in the reality the film thickness reaches values that can allow a turbulent boundary layer to develop, then this model is not reliable any more. In this case the volume of fluid should be properly discretized and traditionally resolved.

- The film stays attached to wall unless another model is added. This means that, in the case of interest, for example, a film stripping model has to be properly specified. This will be examined further on.
- The velocity profile across the film is parabolic. In particular, if ψ is the local coordinate normal to the wall, then the velocity profile is expressed as:

  $$\mathbf{V}(\psi) = \left(3\frac{\overline{V}_f}{h_f} - \frac{\tau_{fs}}{2\mu}\right)\psi - \left(3\frac{\overline{V}_f}{2h_f^2} - \frac{3\tau_{fs}}{4\mu h_f^2}\right)\psi^2 \tag{3.25}$$

  where $\overline{V}_f$ is the average film velocity, τ_{fs} is the shear stress applied on the free surface (that is the one in contact with air), μ is the viscosity of the water (or whatever the fluid film is made of) and h_f is the local film thickness.
- The simulation must be transient. This is due to the fact that the film fluid needs time to grow and develop. A stationary simulation would struggle to give some reliable results, given that that film itself always tends to spread on the surface. Moreover, in case the film occupies all the surface available, its thickness would keep increasing in time, and this fact is not suitable with a steady-state simulation. Plus, stripping of water droplets is always an unsteady phenomenon. So a steady simulation is not compatible when this model is activated.

The fluid film is governed by a mass conservation equation and by a momentum conservation equation. The first one is expressed as follows:

$$\frac{\partial \rho_f}{\partial t} + \nabla \cdot (\rho_f \mathbf{V}_f) = \frac{q_m}{h_f} \tag{3.26}$$

In the previous equation ρ_f is the fluid density (usually assumed constant, as in the case of water) and q_m is an eventual mass source or sink per unit area. This equation is solved for the fluid film thickness h_f. It is important to point out that when equation 3.26 is discretized, some of its terms are multiplied by the cell volume. As mentioned before, the "virtual" cell for this model can be seen as a solid whose base is the face of the actual cell that lies on the wall where the film is computed. The height of this solid is the fluid film thickness h_f, that is unknown. As a consequence of that, when the discretized equation is being resolved, h_f is found in more terms than in equation 3.26. Then, the term q_m takes into account mass that is leaving or joining the film, that is stripping or impingement. The momentum conservation equation is then written:

$$\frac{\partial(\rho_f \mathbf{V}_f)}{\partial t} + \nabla \cdot (\rho_f \mathbf{V}_f \mathbf{V}_f) = -\nabla p + \nabla \cdot \mathbf{T} + \rho_f f_f + \frac{\mathbf{Q}_m}{h_f} \tag{3.27}$$

where f_f is a generic external force acting on the fluid (such as gravity), and $\mathbf{Q}_m$ is the eventual source or sink of momentum corresponding to the mass source or sink q_m (that is impinging or stripping mass with its momentum). $\mathbf{T}$ is the viscous stress tensor within the film. Here is where the shear stress made by the background phase on the film free surface is taken into account. Given that velocity is given by equation 3.25, the momentum conservation equation is solved for the pressure distribution within the film. Again, the term h_f appears in the equation when it is discretized.

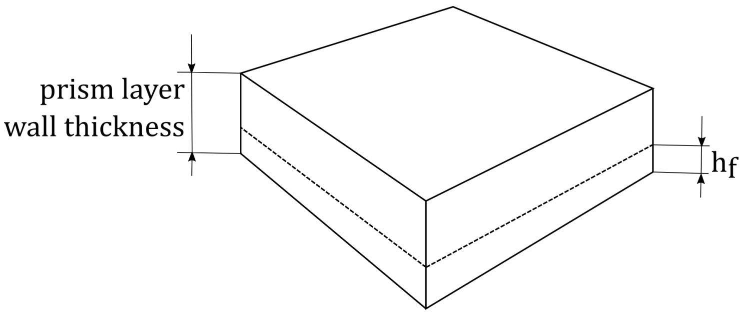

Figure 3.3: A wall cell is showed. Fluid film is calculated in it.

Then, because the fluid film shares an interface (the free surface) with the gas phase outside of it, two boundaries conditions are assumed on this interface. The first one states that velocity of the fluid at the interface must be the same as that of the air in that point. Simply:

$$(\mathbf{V}_f)_{interface} = (\mathbf{V})_{interface} \tag{3.28}$$

The second condition imposed concerns the viscous stress and the pressure forces equilibrium in the boundary-normal direction:

$$(\mathbf{T}_f \cdot d\mathbf{a} + p_f d\mathbf{a})_{interface} = (\mathbf{T} \cdot d\mathbf{a} + p d\mathbf{a})_{interface} \tag{3.29}$$

Where $d\mathbf{a}$ is the area vector normal to the wall. As a consequence of just stated, the film can be seen as mainly driven by two forces: the first one is the gravity force and the second one is the shear force on its surface. If the fluid film on the A-pillar is considered, for example, it will be pushed towards the bonnet and the side of the car by the gravity. On the other hand, the shear force will drag it towards the side window. The prevailing force will therefore lead the movement of the film on the surface. Then, once the velocity, pressure and thickness of the film are calculated, its volume is subtracted from the neighbouring gas cells. In this way the blockage effect done by the film on the free stream is taken into account as well. Having now explained how fluid film is driven, an issue arises when it gets pushed against a wall. When this situation takes place, water is expected to accumulate in that particular place. To avoid having to manage this amount of water, that can be not easy, STAR-CCM+ offers the chance of limiting the fluid film thickness to a certain $h_{f|max}$.

$$h_f < h_{f|max} \tag{3.30}$$

when this height is reached and detected, all of the amount of water that exceeds this limit is removed from the domain, introducing a local (and temporary) sink for the fluid film mass. If this behaviour is not desired, then others models have to be used in order to resolve this kind of water accumulation: one of them is called *Volume of Fluid* (VOF) and it solves the Navier-Stokes equations for the liquid phase. This model could be adequate to find the fluid film solution too, but it has a drawback: it needs its own mesh. This means that, if VOF model is used, all those places where water is expected to form films and to accumulate will need a finer grid. This is the main reason why the Fluid Film model is used instead of the VOF. It is good practise, then, to set the maximum fluid film thickness $h_{f|max}$ equal to the height of the wall cell. If $h_{f|max}$ is greater than this height, then this cell can be found to be entirely occupied by the liquid phase. At this point, it seems reasonable to use a mesh whose first layer has the same height as the maximum fluid thickness. In this way the fluid film can be contained within this layer everywhere. This, though, leads to a high y^+ approach. The fluid film model is now complete, the following subsections will concern impingement and stripping and a brief description of their formulation.

3.4.1 Impingement

The fluid film model is compatible both with the Lagrangian Multiphase model and the Dispersed Multiphase model. So the source/sink terms of equation 3.26 and ref 3.27 are actually source terms when impingement is taken into account. The easiest way to compute the impinging mass is to assume an *inertial impingement.* It means that the mass flux due to impingement is calculated as follows:

$$\dot{m}_k = \rho_f \mathbf{V}_{fk} \cdot \mathbf{A} \alpha_k \tag{3.31}$$

where $\dot{m}_k$ is the impinging mass flux of the dispersed phase in the generic cell k, ρ_f is the density of the droplets, $\mathbf{V}_{fk}$ is the dispersed phase velocity in the cell k, $\mathbf{A}$ is the cell wall area vector (normal to the wall in the outward facing direction) and α_k is the volume fraction if dispersed phase in the cell k. Of course the cell k is the neighbouring cell adjacent to the fluid film. Moreover, the compatibility of this approach with the two multiphase models mentioned before affects the term α_k. If the DMP is used, then α_k is simply equal to the volume fraction calculated for that cell by equation 3.4. On the other hand, if the Lagrangian Multiphase is used, then the volume fraction is obtained staring from the particle diameter. When both models are activated, α_k is the sum of both contributions. So, according to the inertial impingement approach, the mass flux that contributes to the source terms of the fluid film equations is calculated with the normal velocity component with respect to the wall.

This is a very simple way of modelling impingement. However it is sufficient for the purpose of this thesis. In fact, to use a model capable of taking into account more complex effects would increase the computational costs and would slightly increase the accuracy of the results. Such effects that now are neglected are, for example, rebounding or breaking up droplets.

3.4.2 Stripping

Fluid film stripping, that is the separation of a certain amount of mass from the fluid film, can occur in two ways. The first one is called *wave stripping* while the second one is the *edge stripping.*

Wave stripping

As far as wave stripping is concerned, it happens when droplets leave the film free surface as results of the Kelvin-Helmholtz instability. In particular waves develop at the free surface and, as they grow, their instability makes them detach and form cylinders of water just upon the film surface. These cylinders, then, are subject to Rayleigh-Taylor instability, whose result is to break them into different spherical droplets. As reported by STAR-CCM+ user guide [5], this kind of stripping is governed by the resonance wavelength λ_r, that is associated to the waves on the film surface. Its value is a function of the film velocity, of the film surface tension, and of the sum of all inertial and body forces acting on the fluid film. Without developing here all the mathematics of the Rayleigh-Taylor theory, the wave stripping model exploits then an empirical relation that links λ_r to the resulting droplet diameter d. The new droplets are generated with the same velocity as the fluid film. What's more, their initial position is assumed to be a point between the the cell center and the boundary face center, depending on the radius of each droplet. What just stated is enough if the Lagrangian Multiphase model is used to simulate the water droplets. Instead, is the Dispersed Multiphase model is activated, a volume fraction has to be obtained, but this easily done by computing the new droplet volume and the volume of the cell where it is generated.

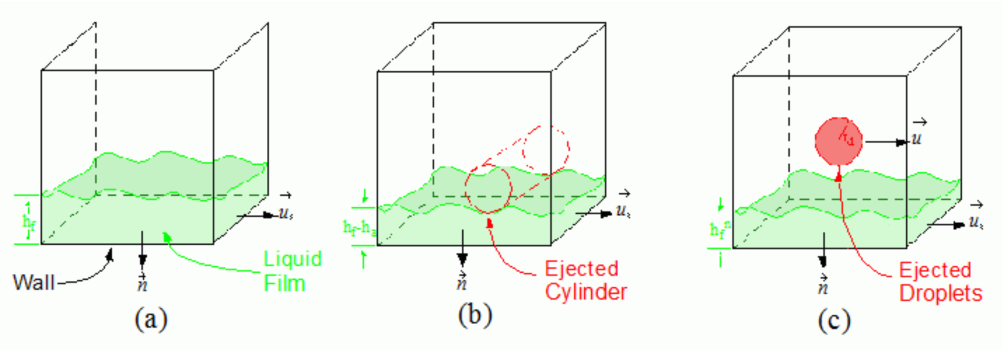

Figure 3.4: The wave stripping mechanism. a) waves are generated on the film surface. b)Kelvin-Helmotz instability takes place. c)Rayleigh-Taylor instability creates new droplets.

Edge stripping

The second type of stripping (i.e. the edge stripping) is the most frequent one. Specially in the case of a vehicle, it is most likely to occur than the the wave stripping because a car has complex geometry, with many sharp edges and angles. The rear spoiler is the one of them, for example, as well as the edges of the rear view mirrors, or the edges of the pillars. In particular the edge stripping is computed where an angle greater of a specified θ_{min} is detected on a boundary. This stripping is governed mainly by one parameter, called the force ratio FR. It is a ratio between the film momentum flux and the contributes of the surface tension and the gravity force. More in details:

$$FR = \frac{We_f}{1 + \frac{1}{\sin\theta} + Bo_f \frac{L_b}{h_f \sin\theta}} \tag{3.32}$$

In equation 3.32 θ is the angle formed by the edge and We_f is the film Weber number. This non-dimensional parameter is ratio of the inertial forces of a fluid to its surface tension. It is defined as:

$$We = \frac{\rho u^2 l}{\sigma} \tag{3.33}$$

where l is a characteristic length, u is the fluid velocity, ρ its density and σ its surface tension. For the fluid film treated here, the Weber number becomes:

$$We_f = \frac{\rho_f u_f^2 h_f}{\sigma} \tag{3.34}$$

Back to equation 3.32, Bo_f is the film Bond number. This parameter is a ratio of gravity to surface tension. It can be expressed as:

$$Bo_f = \frac{\rho_f g_\theta h_f^2}{\sigma} \tag{3.35}$$

where g_θ is the gravity component normal to the downstream wall, that is the wall that comes after the corner. The last term of equation 3.32 to describe is L_b, a dimension that is called the break-up length. This term is given by an empirical relation that takes into account the fluid film Reynolds number Re_f and its relative Weber number We_{rel}. Explicitly:

$$L_b = 0.0388 h_f^{0.5} Re_f^{0.6} We_{rel}^{-0.5} \tag{3.36}$$

$$Re_f = \frac{\rho_f u_f h_f}{\mu_f} \tag{3.37}$$

$$We_{rel} = \frac{h_f \rho (u_g - u_f)}{2\sigma} \tag{3.38}$$

In particular μ_f is the film viscosity, ρ is the density of the gas outside the film (air), and u_g is the velocity component of the gas that is aligned to the first wall (the one before the corner). Now that all the terms have been developed, the edge stripping criterion can now be introduced: stripping is detected when:

$$FR > FR_C \tag{3.39}$$

where FR_C is a critical force ratio. A reasonable and popular break-up criterion is to assume the critical force ratio as unity: $FR_C = 1$. When stripping is detected not all of the mass of the film detaches and leaves the surface. Part of the water will keep being part of the film on the second surface (after the corner). Another empirical expression governs this phenomenon. This expression gives the fraction of fluid film x_f that detaches when it meets the corner. It is:

$$x_f = \begin{cases} 0 & \text{if } FR \leq FR_C \\ 0.44(FR - FR_C) & \text{if } FR_C < FR \leq (FR_C + 1.6) \\ 0.057(FR - FR_C - 1.6) + 0.074 & \text{if } (FR_C + 1.6) < FR \leq (FR_C + 6.792) \\ 1 & \text{if } (FR_C + 6.792) < FR \end{cases} \tag{3.40}$$

Where 1 means full stripping and 0 means that all the film keeps sticking to the wall even after the corner. Again, as well as it happens for the wave stripping, a droplet diameter has to be computed. The mechanism is very similar to the wave stripping one: a wave length is calculated and a diameter is obtained from it trough some empirical relations. So, a droplet for the Lagrangian multiphase model and a volume fraction for the DMP are generated. A particular case of edge stripping occurs when the flow comes from both sides of the edge. In this situation x_f is assumed to be 1 and the droplet diameter is calculated using the properties of the film having the biggest flux.

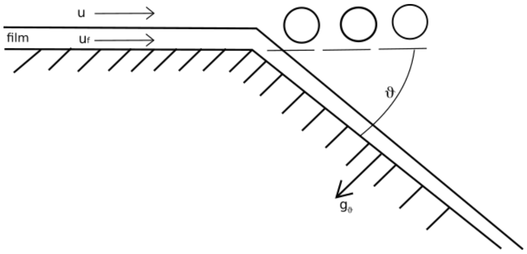

Figure 3.5: Scheme of fluid film edge stripping.

Chapter 4

Vehicle Soiling

This chapter is completely dedicated to the water soiling investigations via numerical simulations using STAR-CMM+. First of all, it is good practise to initialize the flow field around the vehicle, so a section dealing with external aerodynamics comes first. Then there is a section about the choice of rain properties to use in the simulations, followed by another section regarding how water is expected to behave in the A-pillar area. The results will be then discussed in dedicated sections, in particular there is one section for every approach used (DMP, Lagrangian, or a hybrid model). Finally, the results for a very smaller domain (that will be introduced later) are shown and compared to the others.

4.1 Initializing the solution: aerodynamics

In this section it is described how the flow field is initialized: this means that the aerodynamic field around the car has to be solved. As reported by Hagemeier et al. [6], the multiphase models work well when the aerodynamic flow field is already well established. As seen in the previous chapter, the fluid film is sensible to the shear stress that acts on its free surface, so before enabling the Fluid Film model, it makes sense to determine the shear stress on the vehicle. Moreover, especially for the case of the Lagrangian Multiphase model, the air flow field should be well established too. If the Lagrangian Multiphase model is activated when the air flow field is not solved yet, it is easy to imagine that some droplets could follow a completely wrong trajectory. Then, if they impinge on the vehicle, they can give birth to a fluid film development in the wrong place and this can evolve to a point such that the overall solution gets compromised.

4.1.1 Aerodynamics: boundary conditions

In order to execute this aerodynamic simulation, then, no multiphase model is activated. As discussed in the previous chapter, the smallest domain is chosen, so that FCA climatic wind tunnel can be represented. Different types of boundaries (i.e. boundary conditions) are assigned to this domain (see Figure 4.1):

- *inlet*: it is the boundary located in front of the car. Here a *velocity inlet* condition is imposed, that means that trough this boundary the mass of air is allowed to enter the domain with a specified velocity. In particular the velocity chosen for this and all others simulations to come is:

$$V_\infty = 22.22 m/s = 80 km/h \tag{4.1}$$

It is a reasonable speed for the purpose of the simulations. It is very common to drive at that speed, even when it rains, and at the same time it makes the aerodynamic forces not negligible. The direction assumed for the velocity is boundary-normal (entering the domain).

- *outlet*: it is the opposite boundary with respect to the inlet. Here a *pressure outlet* condition in imposed, that means that the ambient pressure ($10^5 Pa$) is assumed on all the boundary surface. What's more, this is the only place where air is allowed to leave the domain.
- *ground*: it is the boundary in charge of simulating the road surface. Therefore it should move with the same velocity as the car is moving. In order to simulate that, a velocity equal to V_∞ is imposed on it. So it has to be said that this particular boundary does not agree with the actual wind tunnel, since FCA climatic wind tunnel does not provide an all-moving floor.
- *side*: it comprehends the three walls that complete the box. They are the two lateral walls and the ceiling. In order to speed up the calculation time, a *slip* condition is imposed on them, which imply that no boundary layer is calculated on these surfaces (indeed no prism layers are generated on them).

To complete the boundary conditions that are assigned to the simulation, all other boundaries are treated as *walls*. On them the velocity is zero and the boundary layer is computed. The last boundary condition that is imposed is a tangential velocity (exactly as it happens for the ground) on the wheels. In particular a coherent rotational speed with the speed of the car is imposed on the surfaces of tires, rims and brake discs, that are the rotating parts of each wheel.

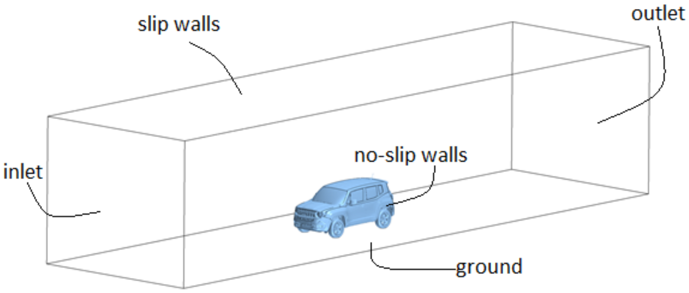

Figure 4.1: Domain and boundary conditions.

4.1.2 Aerodynamics: simulation features

Having set the boundary conditions, an initial solution must be assigned. The initial solution (or initial condition) is the flow field seen by the solver at the first iteration. The more the initial condition is close to the physical solution, the smaller the number of iterations needed to converge will be. Being the final flow field unknown, a velocity equal to V_∞ is assigned to every cell as an initial condition. As far as the type of simulation is concerned, RANS equations are used and the turbulence model exploited is the k-ϵ. The simulation is steady. This practice is proven to work very well for vehicle external aerodynamics simulations. The main difference from a common external aerodynamics simulation, other than the domain size (as seen previously), is the generation of the prism layers (see the best practices reported by [5]). Usually a low y^+ approach is suggested on all the surfaces of the car that are part of its external bodywork, which includes the wind-shield, the side and rear glasses, the bonnet, the bumpers and so on. On these shell fluids film will be calculated, an accurate solution for the wall shear stress would lead to a certain level of accuracy for the fluid film velocity as well. Despite this, as mentioned in the previous chapter, a high y^+ approach has to be used in order to make the fluid film model work properly. In particular the first layer thickness is set equal to $1mm$, that also is the maximum film thickness allowed in the next steps. This is acceptable because the task of this simulation is not determining the drag coefficient of the vehicle (an open air domain would also be better for this aim), but only initialising the flow field for the next step (i.e. the proper soiling simulation). As far as shear stress is concerned, its calculation is helped by the wall functions implemented in STAR-CCM+ (so its accuracy is a bit lower, but it is trusted anyway). Finally, once the simulation is launched, convergence is said to be reached when mass flow trough the engine vane intakes have a constant value through the iterations. This is generally verified after 3000 iterations.

4.1.3 Aerodynamics: results

The results of this external aerodynamic simulations are now analysed. They are very important as they will be the starting point for all the further work. Even tough the solution obtained is not a very accurate one due to the reasons explained before, the main features of the flow field can be observed anyway. First of all, the pressure coefficient is observed on the surface of the Jeep Renegade. It is reminded that the pressure coefficient is defined as:

$$C_p = \frac{p - p_\infty}{\frac{1}{2}\rho V_\infty^2} \tag{4.2}$$

Looking at its distribution, shown in figure 4.2, a stagnation zone is noted on the front bumper and on the license plate. The engine vane intakes are located around this area, in order to exploit this high pressure zone. The exposed parts of the front wheels present a stagnation point as well. Two others high pressure spots are observed on the forward facing side of the mirrors. There is a rapid pressure gradient on their surface as C_p drops proceeding from the centre of the stagnation zone towards any edge of the mirror. It means that, outside of the boundary layer, there is a high velocity zone around the mirror. Almost the same behaviour is seen on the wind-shield, the pressure is higher at its center and lower on its edges. Moreover, another high velocity (low pressure) zone is detected on the A-pillar and on the first part of the roof.

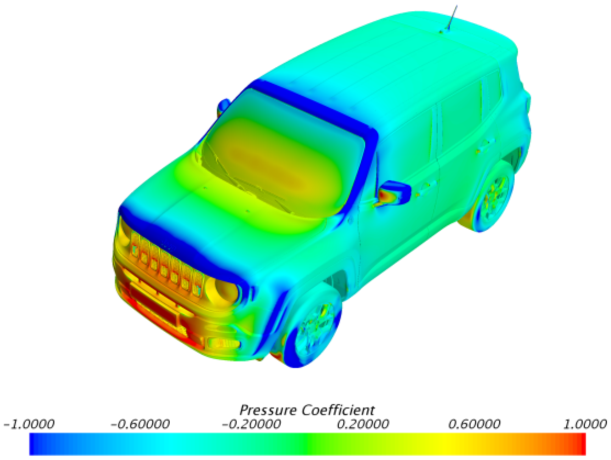

Figure 4.2: Pressure coefficient distribution on the vehicle.

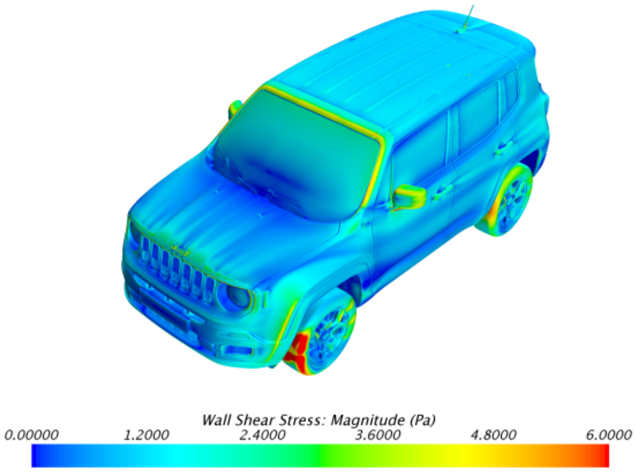

Figure 4.3: Wall shear stress distribution on the vehicle.

The shear stress is checked as well (see figure 4.3). As told before, it can affect the fluid film behaviour in the next steps. The values of shear stress on a road car at conventional speed (such as $80 km/h$) are very low, such that the friction drag consists only of a very small fraction of the overall drag force (about 10%). However it is useful to analyse its distribution in order to estimate where the flow separates from the wall. In facts, where separation occurs, the wall shear stress drops to very low values. This happens, for example, on the rear side of the car. Then, even though it is not very important for the soiling prediction, a picture of the velocity magnitude on the symmetry plane of the vehicle is given in figure 4.4.

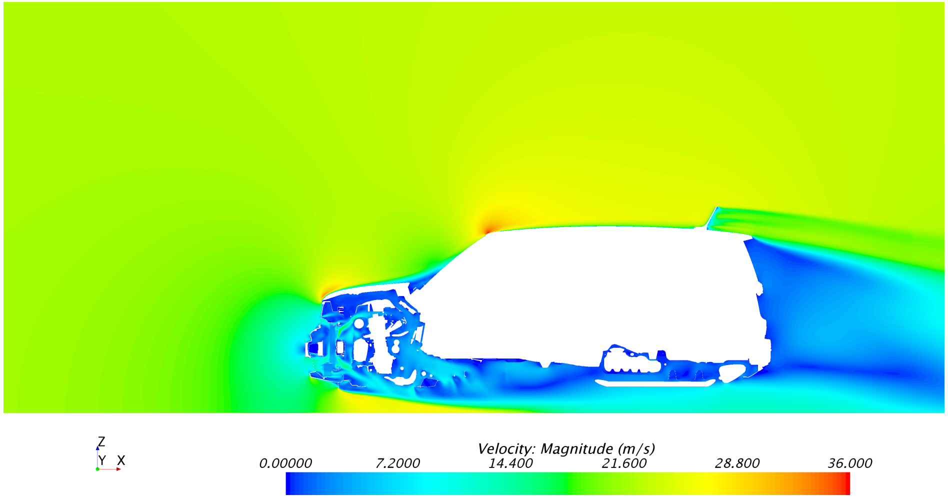

Figure 4.4: Velocity magnitude distribution on the x-z plane.

4.2 Assessing rain properties

Now that a steady solution has been found for the aerodynamic flow field around the vehicle, the proper soiling investigation can begin. First of all, tough, rain properties must be assessed. Given that the DMP model requires a volume fraction to be specified at the inlet of the domain, it is firstly decided to look for this value in literature. Some good values for the the volume fraction α_d can be calculated starting from the numbers reported by Ghani [7] in his article. The liquid water content for different rain intensities (such as light rain, moderate rain, heavy rain and cloudburst) is reported in terms of grams per cubic meter. According this article, 4 to 35 g/m^3 of water are dispersed in the air during a cloudburst. The worst case in terms of rain intensity (i.e. the cloudburst) is selected in order to put the car in the most critical situation it could face. From these values of liquid water content (LWC) the volume fraction can be obtained as:

$$\alpha_d = \frac{LWC}{\rho_{water}} \tag{4.3}$$

where ρ_{water} is the water density ($1000 kg/m^3$). Using the values stated above, the volume fraction stays in the range between $4\ 10^{-6}$ and $3.5\ 10^{-5}$. Being this interval quite large (one order of magnitude), another strategy is chosen. In particular it is decided to obtain the volume fraction from the condition of 100% humidity. When a car is driven behind a heavy vehicle (such as a bus or a lorry), the third part soiling source (that is water raised by other vehicles, see section 3.1) increases and, if the conditions become critical, the quantity of rain contained in the air is not very different from the one that is present in the saturated air. To confirm this, the psychrometric chart (figure 4.5) is consulted: it shows the water/air mass ratio as a function of the air temperature and relative humidity. An ambient temperature of 25°C is assumed and a relative humidity of 100% is selected. With this values the chart gives a ratio equal to 0.023, that corresponds to a volume fraction of:

$$\alpha_{d|0} = 2.3\ 10^{-5} \tag{4.4}$$

It falls within the range found using the data from Ghani [7] for the cloudburst.

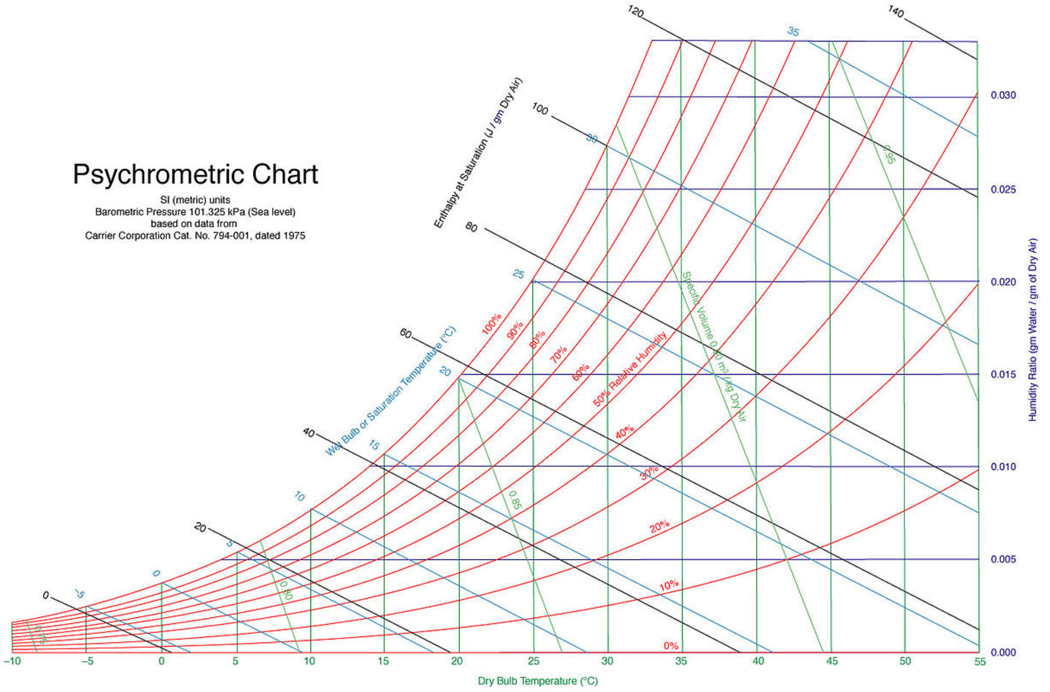

Figure 4.5: The psychrometric chart.

4.3 Soiling: expectations

Before proceeding with the results of the simulations, a bit of attention has to be paid to how water is managed on current road vehicles in order to have a first idea of what to expect from the results. An accurate description of the A-pillar overflow is given by Jilsen et al. [8]. In that article how the A-pillar affects the fluid film behaviour is very well described. In this section the same description is given, but it will be specific for the Jeep Renegade case. The following points, used to describe how water behaves during the A-pillar overflow, refer to figure 4.6.

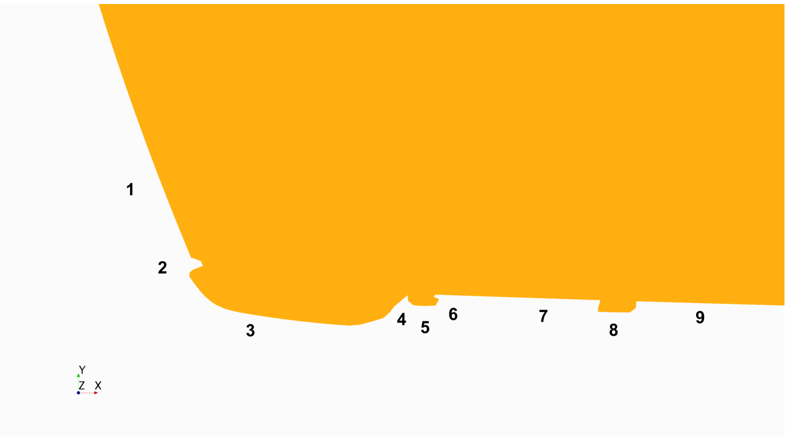

Figure 4.6: Plane section at z=0.9m of the left A-pillar area of Jeep Renegade. Number 1 indicates the windscreen and number 9 indicates the front left side glass of the vehicle.

- *1 - Windscreen*: as confirmed by Jilsen et al. [8], most of the water involved in A-pillar overflow comes from the windscreen. Here water is moved both by wipers (whose effect is not taken into account in this thesis) and by shear forces. As shown by figure 4.8, the streamlines on the windscreen of the car are directed outward, that is towards the A-pillars. To describe it quickly, the direction of the streamlines here looks "radial", even tough this word is not used properly. It is important to point out that these streamlines do not continue on the A-pillar, but, once the reach the side edges of the windscreen, they are trapped by the A-pillar gutter and are deviated towards the roof of the vehicle. Even tough RANS equations are not very efficient in spotting small eddy structures, this phenomenon here is quite evident.

- *2 - A-pillar gutter*: this is the first device used to prevent water film from reaching the side glass. Basically it is a channel located between the windscreen edge and the A-pillar. When water gets over the windscreen edge and enters this channel, it is then driven again by the a force balance. According to the direction of the gutter, water can move upward (toward the roof) or downward (toward the bonnet and the engine vane). Of course the two main contributors to this force balance are the friction force and the gravity force.

- *3 - A-pillar*: the shape of this element can affect the chances of water film reaching the side glass. Some cars may have a sharper pillar or a smoother one. The Jeep Renegade has a quite smooth one, with no sharp angles at all. Moreover, as seen in picture 4.3, the A-pillar is a high shear stress area, which means that it will be very difficult for the amount of water that reaches the pillar to move downwards and drain away. Water is more likely to move upwards or toward the side glass. However, air flow separation is detected at the end of the A-pillar (as shown in Figure 4.7). This implies a drop of the shear stress in the rear side of the pillar.

So, once the fluid film reaches this part of the surface, it is subject only to the gravitational force and the probability it drains downward rises.

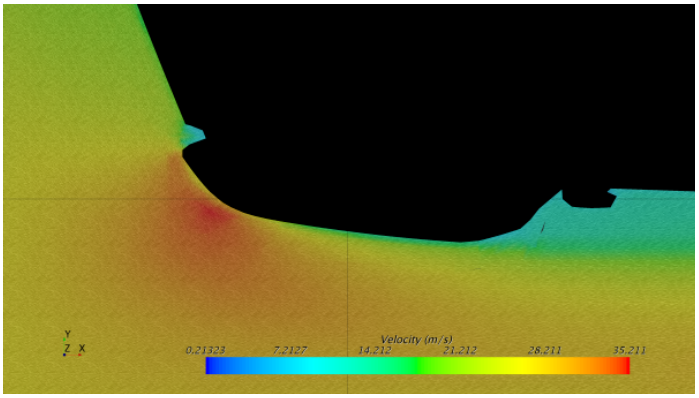

Figure 4.7: Plane section at z=0.9m of the left A-pillar area of Jeep Renegade. Velocity vectors show where separation is detected. Solution obtained with steady RANS equation and k-ϵ turbulence model

- *4 - Door gap*: after the A-pillar, the second big obstacle water encounters is represented by the door gap. It is another channel and water is supposed not to overcome it and to drain away unless critical conditions are applied. Moreover the door gap is in the wake of the A-pillar, so, as explained before, gravity is free to act and pull the amount of water downwards.
- *5/6 - Door seal*: after the door gap channel water has to overcome the door seal, which can be seen simply as a step to climb. So, a relevant amount of water has to be expected on its forward facing side, that is the side of door gap channel seen before.
- *7/8 - Side glass frame*: the Jeep Renegade front side glass has a particular configuration. In fact its front side glass is split into two parts: the front and the rear one. The most important part is the second one, as it is the one trough which the driver can see outside and look at the rear view mirror. The frame that is interposed between the two parts is the last obstacle that water has to face before being free to spread on the second glass. Again, a relevant amount of water has to be expected on the forward facing side of this frame

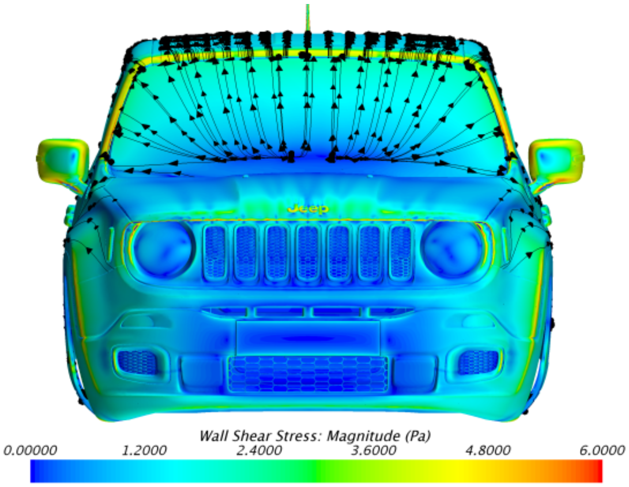

Figure 4.8: Front view. Shear stress distribution and velocity streamlines.

Now that the case has been described, the results will be introduced in the next section.

4.4 Soiling: results - using the DMP Model

4.4.1 DMP: set-up

The first attempt made in order to investigate soiling phenomena is made with the use of both the DMP model and the Fluid Film model. In particular, mass and momentum exchange between the dispersed phase and the film are modelled trough inertial impingement, wave stripping and edge stripping. As mentioned in the previous sections, when the DMP model is used, a volume fraction of dispersed phase has to be assigned to the domain inlet. So the value found in equation 4.4 is specified here. Then, when the fluid film model is activated, the surfaces on which it is calculated have to be specified as well. In order to speed up the calculation time, not all the surfaces of the domain are selected. In particular, given that the area of interest is made by the side glass and the rear view mirror, only the external surfaces of the car are selected for fluid film calculation. Moreover, to increase numerical stability, surfaces of complex geometry or that are located in critical position are removed by this selection. An example of this kind of surfaces is given by those belonging to the front part of the vehicle: the intake grids have a very complex geometry, and the computation of fluid film on them would require too much effort and could lead to important numerical instabilities. They and all of the surrounding parts (such as the license plate, the bumper and so on) are near the stagnation point, that means that they are expected to be highly exposed to the incoming dispersed phase. Hence, according to how the inertial impingement works (see Chapter 3), almost all of the incoming water would become part of the film on these surfaces and could become difficult to manage. Moreover, it is easy to imagine that on such a geometry the calculation of edge stripping phenomena can be very difficult and expensive as well. Many angles and corners are present on such surfaces (especially onthe front grids) and stripping and re-impingement phenomena would complicate quite a lot the computation of the solution without being relevant for the target of the simulation. In conclusion, the boundaries assigned to the fluid film are the bonnet, the glasses, the roof, the rear-view mirrors, the sides and the doors of the Jeep Renegade.

The simulation uses the URANS equations, starting from the steady solution described in section 4.1. Two important parameters that have to be specified when facing a URANS simulation are the time-step Δt and the number of internal iterations. The time-step is strictly correlated to the overall physical time to simulate and to the computational resources available. Investigating the soiling phenomenon also means to check whether it becomes stationary or not. According to Jilesen [8] this phenomenon reaches a quasi-steady state after more than $20s$. So a first overall physical time of $25s$ is chosen:

$$t_{tot} = 25s \tag{4.5}$$

This value of t_{tot} is very high. As a consequence of this, the time-step Δt should be high as well, in order not to spend an excessive amount of time in waiting for the results. On the other hand, a smaller time-step increases the level of accuracy: the more the simulation time-step is closer to the time scale of an eddy, the more that eddy is more likely to be resolved properly (if the size of the mesh is small enough). So the time-step chosen is a compromise between accuracy and calculation speed. It is chosen:

$$\Delta t = 0.0025s \tag{4.6}$$

To make sure that convergence is reached at every time-step the number of internal iterations set is equal to 10. As convergence criteria for the internal iterations it is chosen to check if the continuity and momentum equations residuals drop at least by one order of magnitude. This values of time-step and number of internal iterations allow acceptable run times: as mentioned in Chapter 2, the mesh accounts for more than 90 million cells, so this simulation takes almost 48 hours to complete all of the physical time assigned. The simulation is carried on with 336 processors. A first attempt is done with the k-ϵ turbulence model, and then second attempt is made with the k-ω turbulence model

4.4.2 DMP: results (k-ϵ turbulence model)

During the simulation, fluid film thickness distribution is monitored on the car. Fluid film is detected to start growing on the vehicle after almost 1.5s of physical time. This is the time required by the dispersed phase to travel from the domain inlet to the car. At this time the areas that first get in contact with water (despite the front parts of the vehicle that are not included in the fluid film shell) are the bonnet, the wind-screen, the A-pillars, the upper edge of the wind screen and the forward facing sides of the rear view mirrors. As time goes on, fluid film is generated on these areas and it is driven backwards by the shear forces. From the upper edge of the wind screen, water is pushed onto the roof of the car. Its behaviour on this part of the vehicle is affected by the shape of the roof itself, in fact its ribs help water to move in the x direction. Then, after 3.5s, two main phenomena in the area of interest are noticed:

- a noticeable overflow from the roof toward the front left glass
- a rivulet on the forward part of the door that is originated by the door seal (as expected and described in the previous section).

More in details, this amount of water that comes down from the roof on the side glass, gets spread by the shear forces. As a result, after some seconds, the upper part of the side glass is covered with a thin a layer of water. Fluid film thickness distribution after 5s is showed in picture 4.9, while Figures 4.10 and 4.11 show the solution after 25s. It important to point out that the phenomenon becomes almost stationary (in the area of interest) after 12s.

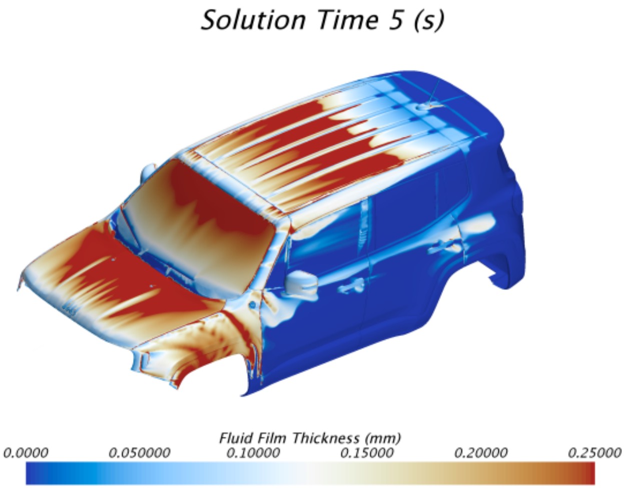

Figure 4.9: Fluid film thickness distribution after 5s of physical time. The DMP model is used. The scale is cut at 0.25mm in order to point out what happens on the A-pillar and on the side glass. Brown areas can exceed the scale up to 1mm. Three location of water overflow can be seen on the A-pillar. The highest one causes water to accumulate in the gap between A-pillar and roof, and then to fall on the side glass.

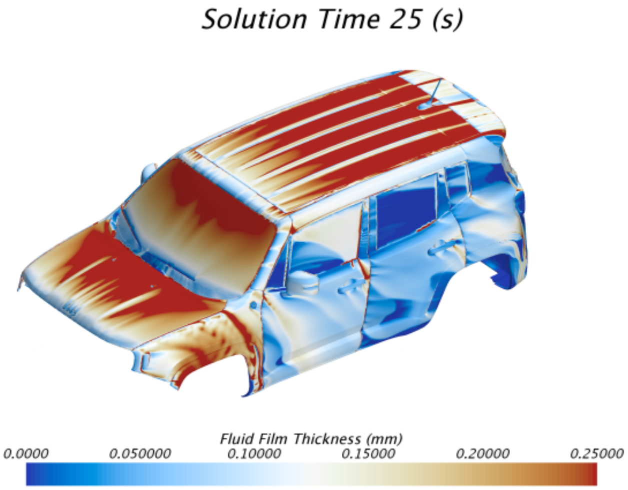

Figure 4.10: Fluid film thickness distribution after 25s of physical time. The DMP model is used.

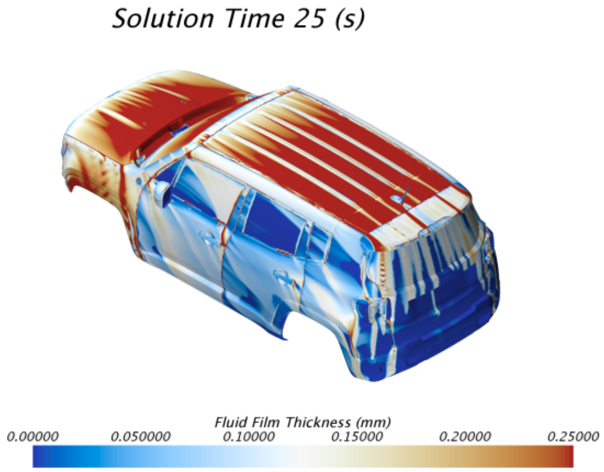

Figure 4.11: Fluid film thickness distribution after 25s of physical time. The DMP model is used.

As far as visibility is concerned, the side glass is partially covered with water. As told before, This layer of water is originated by the amount of water that accumulates in the gap between the A-pillar and the roof. A rivulet starts in this point and moves downwards on the side glass. Here water is pushed backwards and spread on the glass. As time moves on, this water encounters the B-pillar surface and accumulates against it. Exactly as it happens for the A-pillar/door gap, another rivulet on the door is created here and is pulled down by gravity. So, when a steady state is reached, water has found a new path that crosses the glass from its upper left corner to its lower right one. Finally, there is no issue linked to the rear view mirror. It has to be remembered that water distribution given by the DMP approach should be seen as a probability to find water in a particular point. Finally, picture 4.12 shows the impingement rate on the car: the areas hit by rain mentioned before are now highlighted.

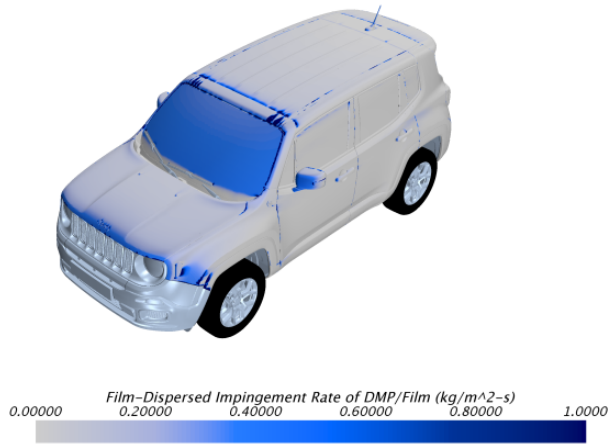

Figure 4.12: Fluid film impingement rate at $t = 25s$. The DMP model is used.

In order to have a better understanding of the simulation just run, some results can be obtained taking a look at the dispersed phase away from the car. If the volume fraction of the dispersed phase is checked on the symmetry plane of the car ($y = 0$), the effect of gravity is clearly visible. Looking at picture 4.13, water enters from the left (the domain inlet) and then it starts falling toward the ground. This behaviour is strongly affected by the droplet diameter imposed ($d = 1mm$). The more the diameter d is bigger, the more the droplet is affected by drag force (as discussed in Chapter 3), and, as a result, it falls sooner. The maximum of volume fraction is reached on the ground and on the stagnation area in front of the vehicle. Here water accumulates, but the Fluid Film model is not activated on these surfaces. So the amount of water that makes α_d (the volume fraction) overtake the limit allowed is removed from the domain.

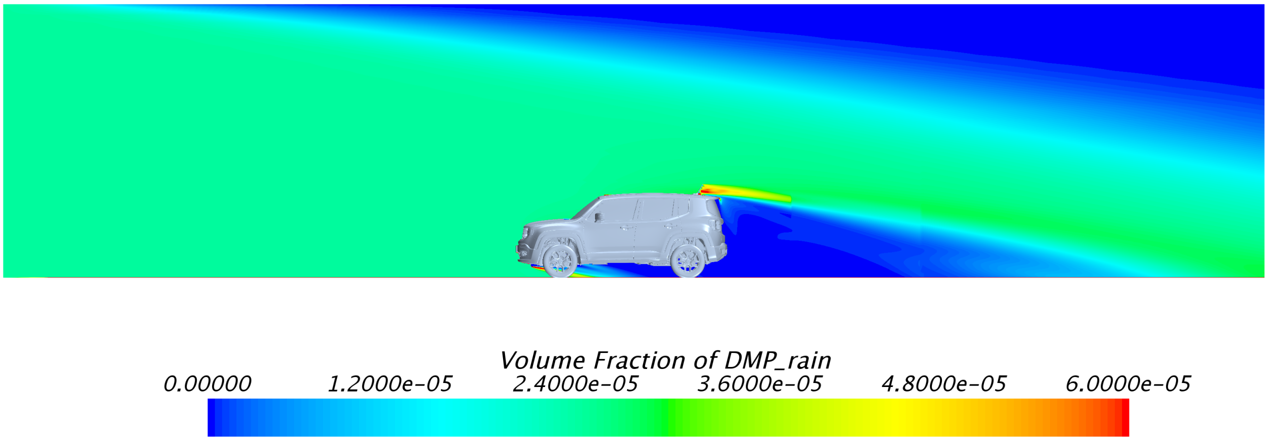

Figure 4.13: Volume fraction of water after 25s. The DMP model is used.

The considerations done about the Stokes number at the beginning of Chapter 3 can be confirmed as well. In fact Figure 4.14 shows both streamlines of air and of dispersed phase. As it is easy to see, water has a very different behaviour with respect to air. This confirms the calculation of the Stokes number done before: they predicted the behaviour of water to be only partially affected by air. What's more, the incidence angle of the droplets can be calculated from the dispersed phase velocity components measured $2m$ upstream of the vehicle. It is equal to 16 deg. This value is sensible to velocity of the background phase and to the droplet diameter: the former make it reduce while the latter makes it increase.

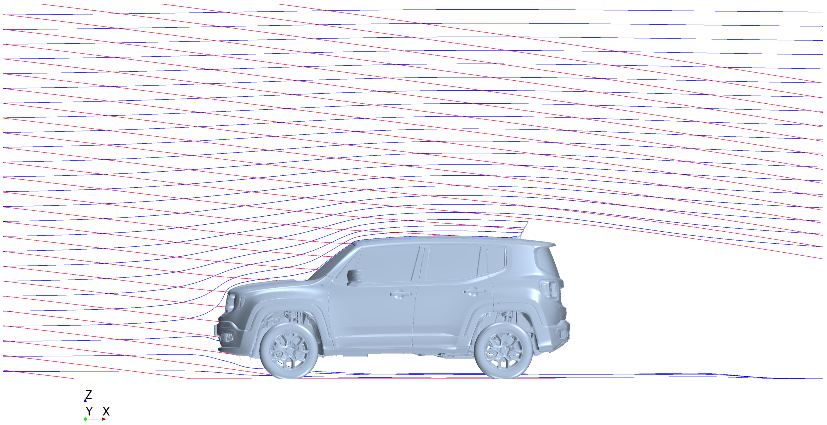

Figure 4.14: Constrained streamlines on the $y = 0$ plane. Red streamlines belong to water, blue streamlines belong to air.

4.4.3 DMP: results (k-ω turbulence model)

The simulation is then repeated using the k-ω turbulence model. As mentioned before, this model can be unreliable if not accurately set-up. Fluid film growth is monitored again on the surface of the car, but this time its behaviour is quite different from the one seen in the previous subsection. What's more the phenomenon becomes stationary after $10s$ of physical time. This leads to the choice of stopping the simulation at $17s$. As showed by Figure 4.15, at this instant the situation is very different from what shown before. The side glass is only wetted in its highest part and the film thickness here is much lower.

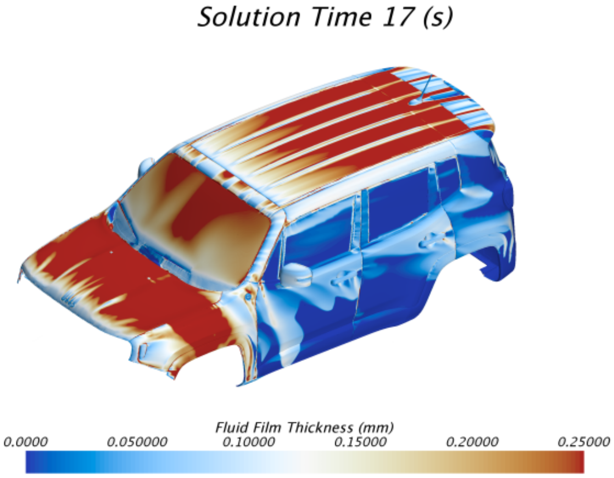

Figure 4.15: Fluid film thickness distribution after $17s$. The DMP model is used. The background flow is resolved with the k-ω turbulence model.

A reason for this important difference with respect to the results shown in the previous subsection has now to be found. First of all, it has to be said that the residuals for the two k-ω variables have a very oscillating trend (even for an unsteady simulation). Moreover, Figure 4.15 shows that the water distribution on the wind screen is not symmetric, as expected and shown by solution obtained with the k-ϵ model. This phenomenon and the lack of convergence in the trend of the residuals are two signals that the solver is struggling to reach an accurate solution. The reason can probably be found in the mesh. In fact, the k-ω could work better with a finer mesh in the boundary layer. It has to be remembered that the first layer thickness is equal to $1mm$ because of the Fluid Film model. Given that the k-ω turbulence model is generally less stable with respect to the k-ϵ, its wall functions used by STAR-CCM+ probably work better with a better near-wall resolution. For this reason, the k-ω model has to be trusted less with respect to the other.

4.5 Soiling: results - using a hybrid model

The same simulation is now repeated with a different setting for the multiphase models. In particular now both edge and wave stripping are set to be sources for Lagrangian parcels, as described in chapter 3. As a consequence of that, Lagrangian parcels can be created only on the surfaces on which fluid film calculation is activated. As far as the background phase is regarded, the k-ϵ turbulence model is used. In this case fluid film thickness distribution is expected to have really few changes with respect to the case seen before (section 4.4.2), given that the incoming dispersed phase is still simulated with the DMP model and with the k-ϵ turbulence model. The drawback of using this kind of set-up is the huge number of Lagrangian parcels generated. They have to be tracked one by one, and this sensibly increases the computational time. As a consequence of that, the simulation is stopped at a physical time of $2s$ after more than 24 hours of run time. The solution at this instant is given by Figures 4.16. In particular, more than 100000 parcels have been generated in this time. As it is evident from the side view, a certain amount of parcels strips from the front edge of the bonnet, but the greatest amount of droplets is detected to strip from the rear-view mirrors. Some of them re-impinge on the vehicle, since there are some spots of fluid film thickness on glasses that were not detected by previous case (section 4.4.2).

However, this kind of approach provides few information more with resect to all-DMP case, at the cost of a much greater calculation time. So it can be useful only to spot where stripping locally occurs. As far as a common road vehicle is regarded, water stripping locations are quite predictable because edge stripping is dominant with respect to wave stripping, as it can be seen from the droplets trajectories. Moreover, if the diameter of these droplets is checked, a critical observation needs to be done. Figure4.17 shows the distribution of the diameters of the droplets. In particular, the majority of these droplets has a diameter equal to $0.3mm$. This is quite in accordance with what reported by Gaylard [9]. In this article is reported a dominant droplet size of $0.1mm$. In particular they are registered for the wake of a lorry 50 meters behind it (third part soiling).

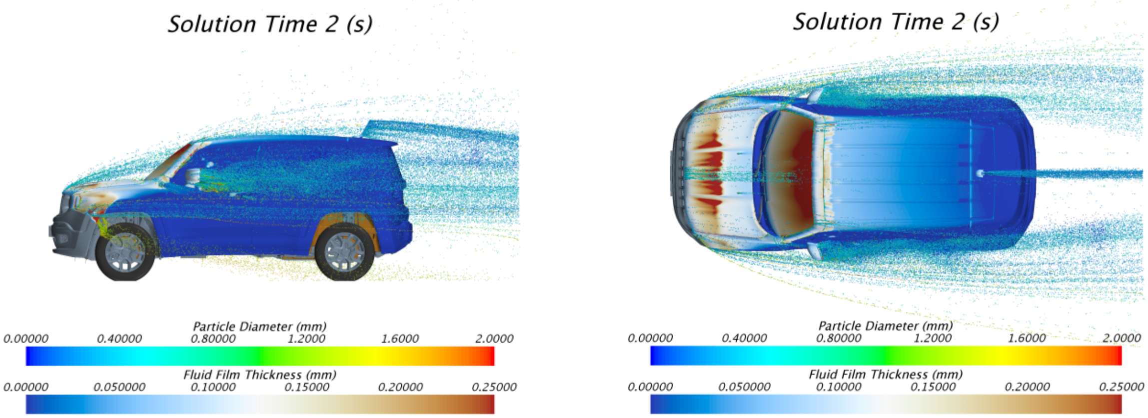

Figure 4.16: Fluid film thickness distribution at $t = 10s$ and stripping droplets diameter. The DMP model is used for the incoming water. Stripping droplets are modelled with Lagrangian Multiphase model.

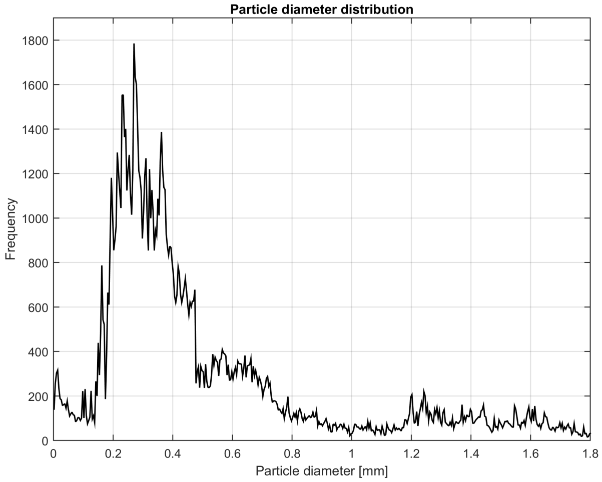

Figure 4.17: Stripping droplet diameter distribution.

4.6 Soiling: results - using the Lagrangian Multiphase model

An alternative to the Dispersed Multiphase model is the Lagrangian Multiphase model. As seen before, this model becomes quite slow when it comes to managing a large number of parcels. So, a trade off between a fast simulation and a proper number of parcels has to be found. In this section then simulation set-up is firstly reported and then the results obtained with this method are shown. Again, the flow field in initialized with a steady state RANS simulation (the same used for the previous cases).

4.6.1 Lagrangian Multiphase: set-up

To simulate water behaviour in a rainy day in the wake of a lorry, for example, a lot of particles (and so a lot of parcels) are needed. In order to simplify the computation and to save some time, the first decision taken is to exploit the property of Lagrangian Multiphase solver of receiving some coordinates as input and placing a source there. As a consequence, only a specific area of interest can be set to be subject to water spraying. In this way the computation of the behaviour of the water phase can be avoided in certain areas (such as the under hood). More in details, a matrix of points that act as sources can be placed in front of the vehicle, and in particular in front of the A-pillar and right the left rear view mirror, as shown in figure 4.18. Each point is a source of Lagrangian parcels. In this way the number of droplets generated can be a relatively small and water can entirely be oriented toward the A-pillar area. Here, to be coherent with the DMP case, the amount of incoming water should be as uniform as possible.

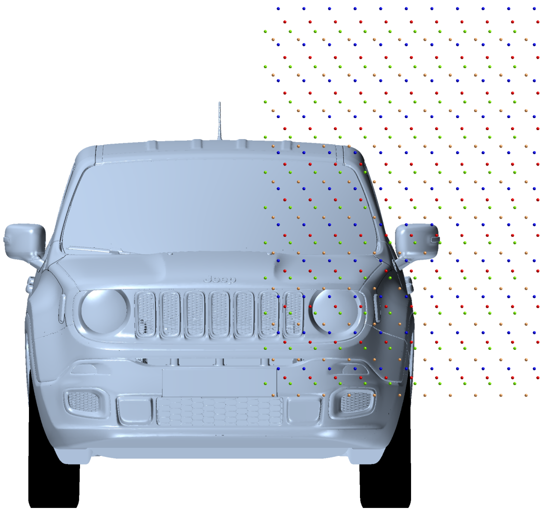

Figure 4.18: Location of the points matrices used as source for Lagrangian parcels. The matrices are located $2m$ upstream of the vehicle. Here four matrices (one per colour) lie on the same plane ($x = -2m$), and their points are equally spaced.

After several tries, a good compromise for setting up the simulation is found with the following parameters for the injectors points:

- a first 10x10 injector matrix: 100 injectors that work with a *parcel stream* parameter equal to 1, this means that one parcel is generated per point per time-step.
- The time-step for URANS equations is $\Delta t = 0.0025s$. This combination of number of injectors, time-step and parcel stream allows both an acceptable run time and a reasonable accuracy.
- The matrix lies on the $x = -2m$ (which means $2m$ upstream of the front axle of the vehicle vehicle).
- The matrix is made of 100 points. These points have a constant distance in y direction and another constant one in z direction. Moreover, they represent a rectangle whose dimensions are: $\Delta y = 1.30m$ and $\Delta z = 1.80m$.
- In order to avoid having constant impingement location points on the surface of the car, other three different matrices are created. They all stay in the $x = -2m$ and they are still part of the rectangle represented by the first matrix. Despite this, tough, the four matrices are

misaligned with respect to each other (as shown by Figure 4.18). By doing this, 400 points are displaced in front of the Jeep Renegade.

- A step function with respect to time is assigned to every matrix so that they turn on alternatively. In this way the number of injector points active at the same time is never greater than 100.
- A mass flow must be assigned to these matrices. Given that the flow field is initialised with a steady solution, air mass flow is measured across the rectangle mentioned in the previous points and the value obtained is $\dot{m}_{rect} = 50kg/s$. To be coherent with what done before (see section 4.2), according to figure 4.5, water mass flow across this section is equal to:

  $$\dot{m}_{W-rect} = 0.02\dot{m}_{rect} = 1kg/s \tag{4.7}$$

  This is the value assigned as peak value of the step functions mentioned above. Once the mass flow is assigned, it is divided between all the parcels created per unit of time.
- Every parcel created by the four matrices is set to be born with same velocity of air in that point.
- Finally the particle diameter is assigned: it is chosen to set it equal to $1mm$.
- In order to get rid of redundant droplets, those whose position is far from the area of interest are removed from the domain. This helps speeding up the calculation.
- Fluid film is set-up is exactly the same as used for the DMP case.
- To further lighten the model, parcel depletion is active on all the surfaces that are not part of the fluid film shell, which means that a parcel that contacts one of these surfaces gets deleted. Impingement on the fluid film shell is again modelled with an inertial impingement. Edge and wave stripping are used again.

Now that the Lagrangian Multiphase solver has been set, it is ready to run coupled with the usual aerodynamic models. In particular URANS equations are used (as mentioned before) with the k-ϵ turbulence model. Gravity is considered as well.

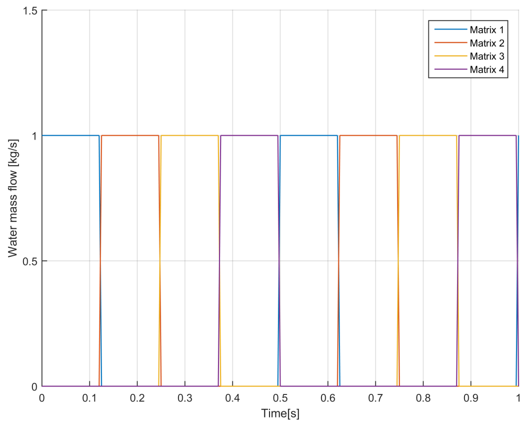

Figure 4.19: Step function used to define water mass flow for the Lagrangian phase. Each color corresponds to an injector matrix.

4.6.2 Lagrangian Multiphase: results

This kind of simulation takes more time to run compared to the DMP case. In fact, to complete a total physical time of $\Delta t = 10s$, more than 48 hours are needed. In order to have a comparison with the hybrid model seen in section 4.5, after 10s, 32573 parcels are present in the domain, that is 1/3 of the droplets generated in the hybrid simulation. The reason of this fact lies within the choice of wetting only a portion of the car. Again, fluid film thickness distribution is monitored as time goes on. Since water is generated much closer to the car, impingement is detected to happen in less than $1s$. In particular, when a particular matrix is active, impingement locations on the left part of the the wind-screen are coincident with the projection of the injector points on it. This confirms that the choice of using alternating sets of points as sources is right. In fact, as soon as another matrix is enabled and its parcels reach the car, fluid film thickness distribution rapidly changes and tends to a more uniform distribution, that looks more realistic, since rain is a random phenomenon. Moreover this way to operate is more similar to what done in the DMP simulation. Of course the area that gets wetted is only the area of interest: A-pillar, front left glass, left rear view mirror and their neighbours, such as the left part of the wind screen just mentioned.

As time moves on, water spreads on the roof (following the shape of its frames) and, as it happens for the DMP case, it falls on the glass from its upper left corner. In terms of visibility, the phenomenon is similar to what seen for the DMP case: the upper side of the glass is partially covered with water. This phenomenon can affect lateral visibility or can prevent the driver from seeing the rear view mirror. This amount of water then ends up on the lower edge of the glass. After $10s$, the situation is given by Figures 4.20 and 4.21:

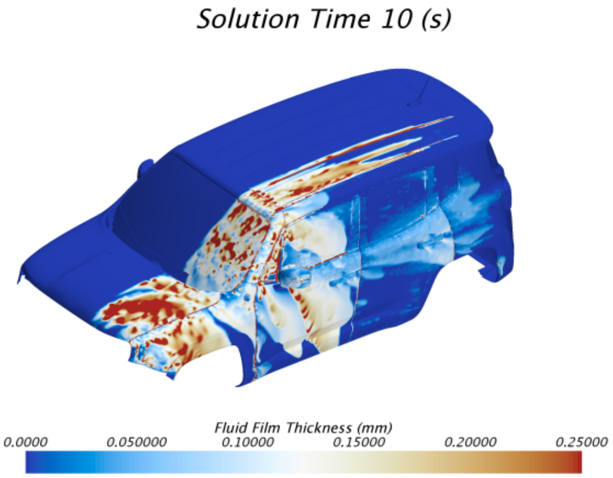

Figure 4.20: Fluid film thickness distribution after 10s. The Lagrangian Multiphase solver is used. Water falls on the side glass from its top left corner as seen in the DMP case. Despite this, though, fluid film develops on the forward part of the glass too.

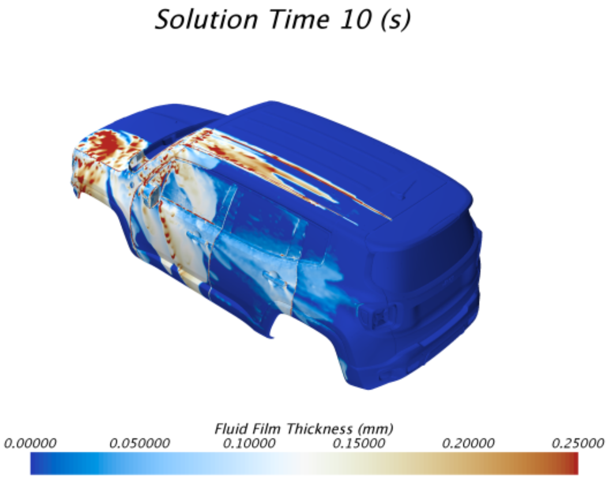

Figure 4.21: Fluid film thickness distribution after 10s. The Lagrangian Multiphase solver is used.

Both Figures 4.20 and 4.21 have to be compared with Figures 4.10 and 4.11. Even tough they refer to a different solution time, some phenomena can be seen to happen in both the simulations. For example, the rivulet that falls from the gap between the A-pillar and the door is very similar between the two results. As told before, the side glass is wetted form the upper left corner in both cases. However, a great difference is seen on the forward part of the glass (the triangular part). According to the DMP results, this part of the vehicle is not wetted, while according to the Lagrangian Multiphase model simulation, it is. Moreover, in the latter case, water is then accumulated against the glass frame and gives birth to another rivulet on the central part of the door.

If the rear view mirror is checked, no great difference is noticed, but how water interacts with its wake is quite different. In particular, the effect of stripping droplets is much more evident using the Lagrangian Multiphase model. In fact, the thin spots of fluid film thickness on the rear door and glass can be the result of re-impinging droplets that come from the mirror. Then, picture 4.22 gives an idea of how parcels interact with the vehicle.

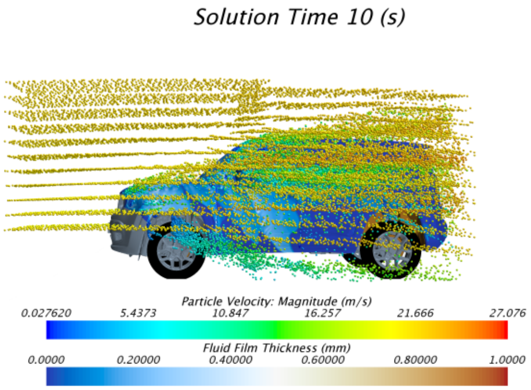

Figure 4.22: Parcels at $t = 10s$. The Lagrangian Multiphase solver is used. The effect of the step functions can be seen on the position of the parcels: the source matrix of the droplets on the right is different from the source of the droplets on the left.

If parcels generated by fluid film stripping are isolated, it can be seen that their number is equal to 16242 (almost half of the total number of parcels currently present in the domain). They are shown in picture 4.23 as already observed in the previous simulation, the main source for water stripping is the rear view mirror. Their diameter distribution is checked as well and it is shown in Figure 4.24. The peak is given for $d = 0.3mm$, not very different from what seen before.

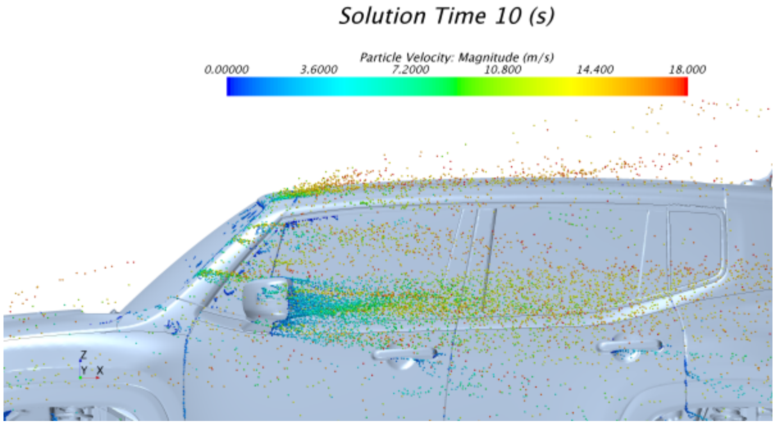

Figure 4.23: Stripping parcels at $t = 10s$. The Lagrangian Multiphase solver is used.

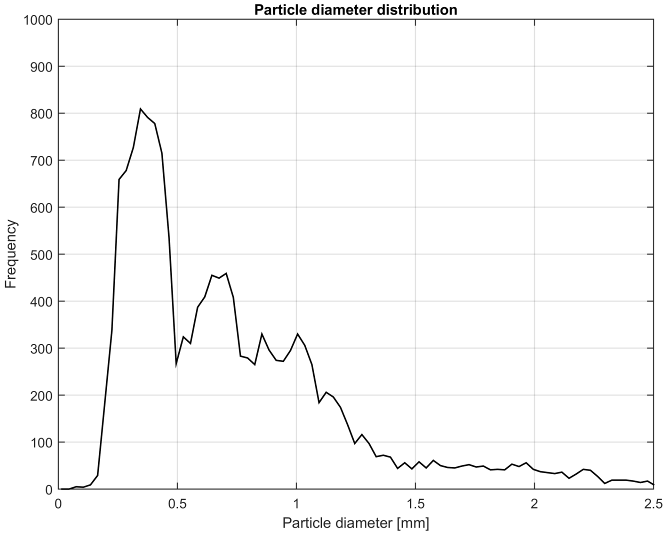

Figure 4.24: Stripping parcels diameter distribution at $t = 10s$.

4.7 Soiling: DES on a reduced domain

4.7.1 Domain choice and simulation set-up

As seen in the previous sections, some small differences are noted between the results obtained with the Lagrangian Multiphase model and the DMP model. In particular, the way water reaches the side glass looks slightly different. In fact the solution provided by the Lagrangian Multiphase model gives a more critical fluid film development on the A-pillar and across the door gap. As a consequence of that, the forward part of the glass gets wetted too. In order to further investigate the phenomenon, it is chosen to attempt a Detached Eddy Simulation (DES, see section 2.2.4). In particular, this kind of simulation is more accurate in catching the background flow motions with respect to time and space. As a consequence of that, it requires a very small time-step. In particular it is chosen $\Delta t = 2.5\ 10^{-4}s$. Therefore, if the same physical time as the previous simulations has to be reached, the number of time-steps required becomes very high and the simulation gets too expensive. For this reason, this attempt is done on a reduced domain. In particular a box is drawn around the A-pillar area, and only what included in it is part of the new domain. The mesh for this domain is generated with the same specifications seen for the whole car domain and it accounts for less than 4 million cells. With such a lower number of cells, the simulation becomes much faster. In particular, it takes only a bit more than 24 hours to complete 25s of physical time running on 336 processors. As far as multiphase models are concerned, Dispersed Multiphase model is chosen since it takes less time to run. Moreover, Fluid Film model is activated on all the shells of the domain except for those belonging to the box. The domain is shown in the Figure 4.25:

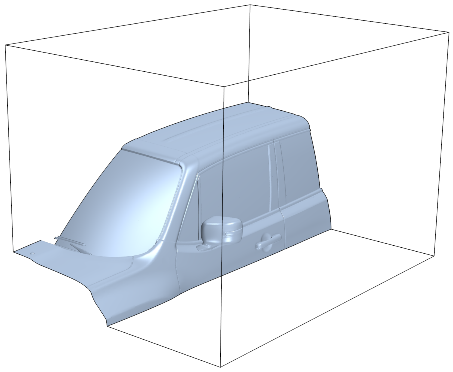

Figure 4.25: Reduced domain chosen for DES.

The biggest problem of setting up such a simulation is represented by the choice of the correct boundary conditions. Given that the boundaries are quite close to the car, this choice can heavily affect the results. The quickest way to assign some boundary conditions to this domain is to map them from a steady state whole vehicle simulation and then to copy them into the new simulation. In particular, the first steady state RANS simulation comprehends the DMP model without the Fluid Film model, since this is the only way to execute a steady state multiphase simulation. So the mean field of both air and dispersed phase is obtained. This flow field is then mapped on all the points belonging to the boundaries of the new smaller domain. The quantities mapped are pressure, air velocity, dispersed phase velocity and volume fraction of the dispersed phase. In particular only the inlet and the outlet of the this new domain are mapped, since all the velocities components normal to the other walls are approximately zero. More in details, mapped air velocity, DMP velocity and volume fraction are assigned to the domain inlet (that is a *velocity inlet*), while the mapped pressure is assigned to the outlet (that is a *pressure outlet*). Moreover, all of the other boundaries that are not part of the car, are set to be *slip walls*. The k-ϵ turbulence model is selected for near wall regions.

4.7.2 DES: results

Unfortunately the results do not agree with those obtained previously, as shown by Figure 4.26. In particular the side glass does not get wetted, and fluid film thickness distribution on the car looks different.

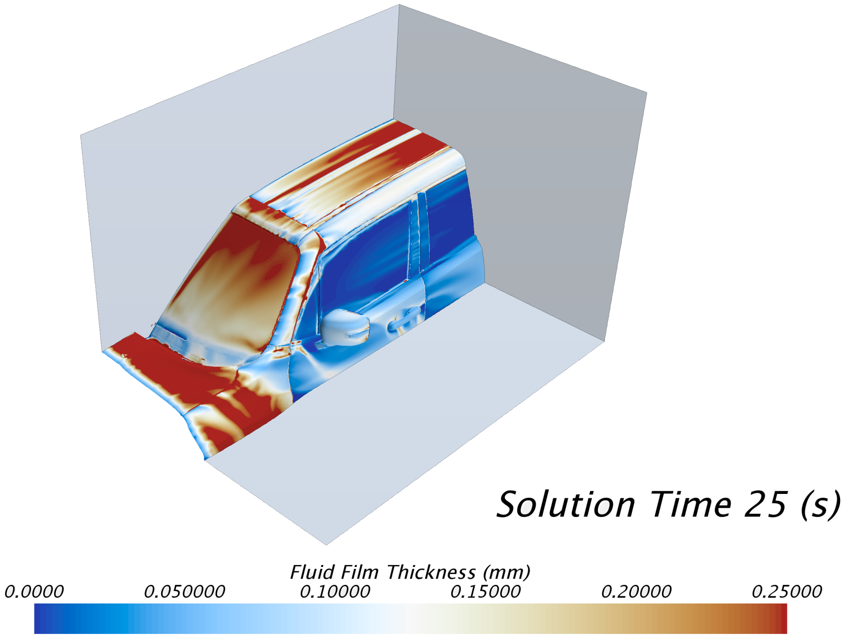

Figure 4.26: DES result: it does not agree with the ones shown previously.

The main reason for this could be the way boundary conditions are assigned. In fact, what done here, is trying to run an unsteady simulation imposing some stationary boundary conditions. Moreover, this is a highly unsteady area and these conditions could be imposed too close to the car. In fact, it is easy to imagine that in the car proximity, the turbulence fluctuations are more intense, and so the flow has an unsteady behaviour. If a wider domain is chosen, probably more stable conditions would be found. The drawback of choosing a wider domain, though, is the increase of the number of cells generated. As mentioned before, to run a DES simulation (with a very small time-step) on a reduced domain takes almost half of the same time as running URANS (with a larger time-step) on the whole car domain. Anyway this is a huge amount of time, given that the number of cells of the reduced domain is equal to only 4.4% of the number of cells of the whole car domain. So, to increase the dimension of the DES domain increases a lot the resources required.

4.8 Soiling: an experimental test

Given the differences seen between the Eulerian and the Lagrangian approaches to the problem and, most of all, between the k-ω and the k-ϵ model, an experimental test is needed as a way to compare the results. Current regulations do not require this kind of test in terms of vehicle homologation. Anyway this test can be performed easily in FCA facilities.

4.8.1 Test set-up

The wind tunnel test takes place at FCA climatic cold wind tunnel. This facility is usually used for testing vehicles in critical conditions, such as very cold temperatures, so this structure is not used to measure the aerodynamic forces because of its smaller section (the blockage effect would compromise these measures). Anyway, as discussed in Chapter 2, the domain used in CFD simulations has the same section as this wind tunnel. As far as the wind tunnel is concerned, its main features are:

- Close return: this kind of wind tunnels are made by one channel (that includes the test section) in which the flow is recirculating. Some turning vanes are located at the four corners in order to ensure a relatively uniform flow in the test section. With the same purpose (and to smooth turbulent fluctuations), some straighteners (made by a honeycomb section) are located before the test section. A fan, then, provides the thrust necessary to win the losses along the wall and through the turning vanes.

- Radiators: even tough they are not relevant for the current test, they are located within the wind tunnel in order to reduce the flow temperature when required and to dissipate the heat generated from the losses.

- Test section: here is where measurements are done. A vehicle can be placed in it and there are some devices to avoid any of its possible displacements. A convergent channel is located before the test section in order to reach the velocity requested in the test section.

Now that a brief description of the wind tunnel has been given, the problem of generating the dispersed phase is faced. The only available device capable of spraying water into the air stream is the one used for the Slipstream test (described in the following Chapter). It is made by four nozzles linked by a pipe trough which comes water. These nozzles can be oriented so that a specific area can get sprayed. Water mass trough this device in known, but it is difficult to link this mass flow to the amount of water used in the numerical simulations because now water is sprayed from a specific point with a certain opening angle, while in CFD simulations there was a uniform advancing front of water. The pipe with its nozzles is adjustable in terms of height from the ground and position with respect to the car, since there are several attachment points available on the floor of the wind tunnel. The position chosen is shown in Figure 4.27. From that position water can reach the area of interest (A-pillar, front left glass and rear-view mirror).

Figure 4.27: Position of the four nozzles during the water soiling experimental test.Courtesy of FCA

Now that a way to recreate the phenomenon has been found, a way to make some measurements should be found. Unfortunately to measure the fluid film thickness or the droplet diameter some dedicated instruments are required. For example, Gaylard [9] mentions a very effective UV technique, but the instruments it requires are not available. Therefore a more qualitative investigation has to be carried on. As showed by Dasarathan and Jilesen [10], qualitative observations can be as well compared with numerical results. As a consequence of that, a camera is located into the wind tunnel in order to record what happens on the A-pillar area. However, to track the water path on the surface of interest, a spray talcum powder is exploited. In particular it is sprayed on the A-pillar, on the rear view mirror, and on the side glass. Once a water rivulet moves onto it, it is supposed to leave a track. In fact water carries the talcum away as it is driven on it. As a result, at the end of the test, water paths are expected to be seen as areas where the talcum powder is missing.

Figure 4.28: Talk is sprayed on the area of interest in order to track the path of water rivulets.

Before spraying the talcum on the car, though, the injectors are manually adjusted in order to be well oriented toward the area of interest. During this operation, due to their close proximity to the car, water jets are detected to lift too much before reaching the car when the win speed is set to 80km/h. To provide a reasonable behaviour of water (more uniform, for example), the nozzle position should be changed into another one that is not allowed by the attachment points on the ground. As a consequence of that, it is decided to execute the test at 50km/h: in this way the water jets do not lift too much and the area of interest of the car gets well wetted.

4.8.2 Test results

All the non-similarities with what done numerically are summed up and listed below:

- Water mass flow is different. The amount of water injected in the wind tunnel is smaller that the one used in CFD simulation with the Lagrangian Multiphase model, for example.
- The way water is injected is different. Even though both the DMP and the Lagrangian Multiphase models have very different ways to deal with sources of dispersed phase, what done in the wind tunnel is still different from these two methods.
- Wind speed is different. This affects the overall Reynolds number of the phenomena.

- Droplet diameter is unknown. There is no way to measure the diameter of the droplets sprayed by the nozzles.

With all these compromises in mind, the test is executed. As mentioned before, the front left glass is monitored. As soon as water is injected, any particular phenomenon is detected. Water impinges on the wind screen and on the rear-view mirror, as expected. It takes two minutes to notice a very interesting phenomenon: water accumulates in the gap between the A-pillar and the roof, few centimetres above the angle of the wind screen. This is showed by Figure 4.29.

Figure 4.29: After two minutes water accumulates in the area highlighted by the circle.

It takes few seconds, then, for water to overcome the A-pillar and to fall on the glass. After one more minute a noticeable amount of water is seen on the glass, and it looks very similar to the numerical results obtained both with the DMP and with the Lagrangian Multiphase models. In particular, there are some rivulets coming from the front part of the glass as well. They overcome the glass frame and join the water that is falling from the roof.

Figure 4.30: After three minutes water has overcome the A-pillar and has fallen on the side glass.

Then, this phenomenon becomes almost stationary, as it happens in the CFD results. Finally, Figure 4.31 shows a closer view of the side glass. This picture was taken after the test and is a prove of how talcum can keep track of water rivulets.

Figure 4.31: The path of water rivulets is tracked by the talcum powder. The picture is taken after the test.

As seen from the previous pictures, the time scales of the phenomenon are quite different from those seen in the numerical simulations. The reason lies in all the compromises listed before. In particular, the amount of water injected into the wind tunnel (in terms of mass flow) is lower than the the one use in the simulations. This could explain why it takes so much time for the glass to be wetted. Probably all the water that falls into the gap between the A-pillar and the roof has few chances of escaping. In fact, if the shear stress is checked here (via CFD, see Figure 4.32), once water reaches this channel, there is a shear stress drop. This means that water is free to accumulate here because this is an horizontal surface, so gravity has no effect on water direction. When the amount of water reaches a critical level, it moves toward the glass and falls on it.

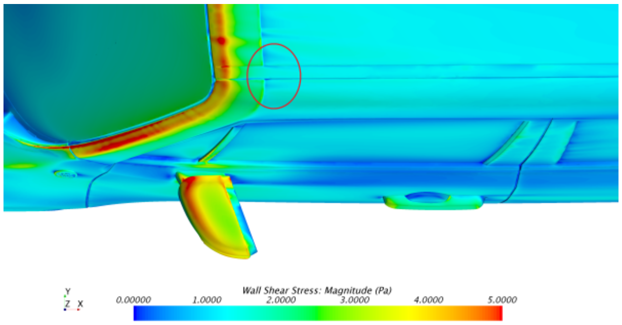

Figure 4.32: Shear stress distribution. The circle highlights where the shear stress drop occurs. Here water accumulates and then falls toward the glass

.

Chapter 5

Engine water ingestion

In this chapter multiphase models are used again, but with a different purpose. This time the target is to investigate how much water is collected by the engine air intake system in case of a lorry water wake in a rainy day. In particular there is specific experimental test for this issue, and in this chapter it will be replicated from the numerical point of view. First, how an engine intake system is made is explained, then the test procedure is reported. After that, how a CFD simulation for a water ingestion test is set is described and finally, in the last two sections of the Chapter, its results are given.

5.1 The air intake system

The engine air intake system is the part of the vehicle in charge of taking the air from the external environment, cleaning it and delivering it to engine cylinders or to the turbo system (if this one is mounted on board). It is very important for the air that takes part to the combustion process to be as dry and clean as possible, in order not to affect the engine efficiency. Here, Jeep Renegade 2.4L Multiair engine is considered. The three main components of the intake system of this vehicle are:

- the *dirty air duct*: it takes the air right behind the front grids of the vehicle and makes it get to the filter box. In particular the first part of this duct is convergent and then its section remains almost constant. It has a certain curvature radius, which can affect the behaviour of water droplets that are travelling trough it. The dirty air duct, then, ends in the lower part of the filter box.

- the *filter box*: it contains the filter, whose task is to remove small dirt particles from the flow. This is usually the place where water gets trapped. On the lower side of the filter box there are three "turning vanes" that help directing the flow towards the filter inlet surface. The filter, whose shape is a parallelepiped, is located in a quite horizontal position (with respect to the ground) and the flow crosses it from its lower face to its upper face, so that gravity can contrast particles that are dispersed in the flow and can help making them fall. An important feature of the filter box is the presence of two drain holes on its lower side, made to drop the accumulated rain and let it fall outside of the box. During the Slipstream test performed at FCA (see next section) these holes are closed in order to actually measure all the water that enters the system, so the same is made on the CAD geometry of the filter box that will be simulated. Then, once air overcomes the filter, it moves through the upper side of the filter box and flows into the clean air duct.

- the *clear air duct*: it is in charge of delivering the air to the turbo system of the 2.4L engine. It is the longest duct of the system (see figure 5.2), and its section is almost constant for all of its length. As far as CFD is concerned, this duct ends at the inlet of the turbo: here a mass flow inlet with a negative mass flow is imposed in order to simulate the air sucked by engine.

The purpose of the filter is to be an obstacle for dust and water. As far as water is concerned, the filter acts as a sponge, since it is made of cotton gauze. Hence, water gets trapped inside it due to the small openings trough which it has to move. Given that the average size of an opening of the filter (if seen as a sponge) is smaller than the average droplet diameter (that is about $1mm$), surface tension forces prevent water from leaving these openings. Then these droplets that are trapped within the filter are subject to gravity and, after some time, they can reach its the lower face. They can detach and then fall into the filter box and its drain holes.

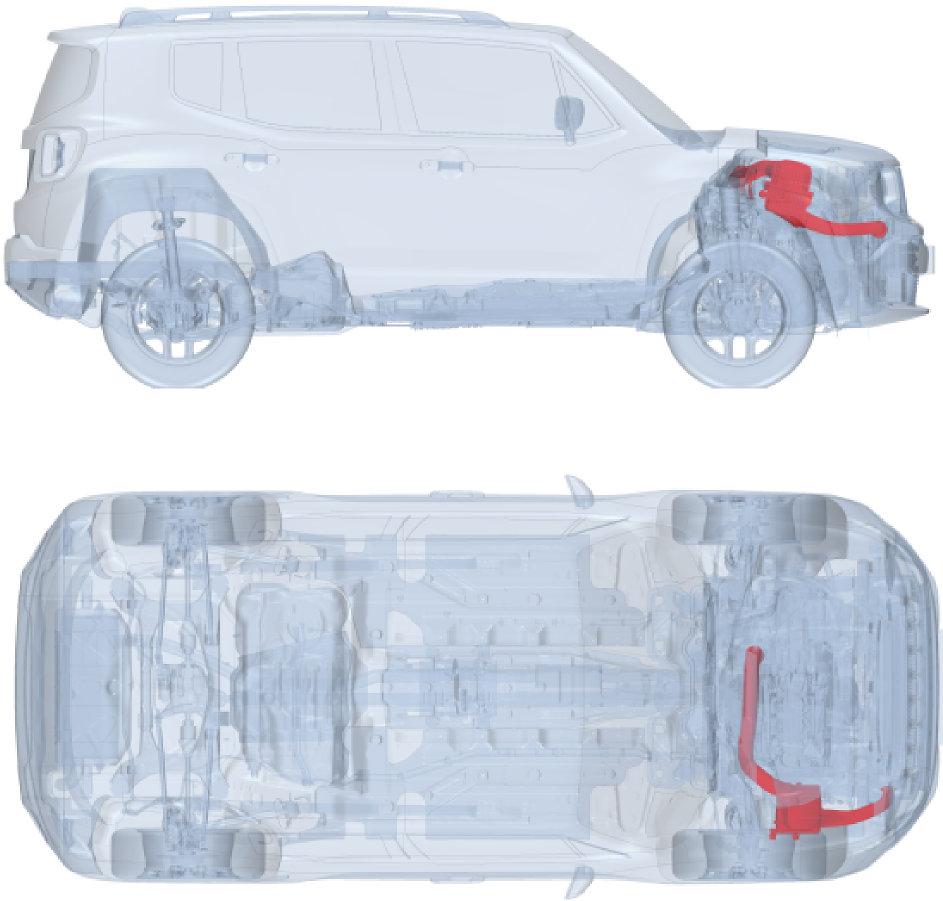

Figure 5.1: Location of the air intake system on the 2.4L engine Jeep Renegade. Side and top view. Courtesy of FCA

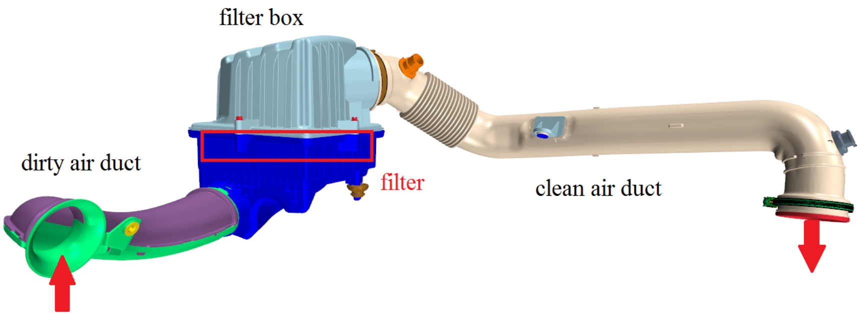

Figure 5.2: CAD model for the air intake system of Jeep Renegade 2.4L Multiair. Courtesy of FCA

5.2 The Slipstream test

The purpose of the Slipstream test performed at FCA is to simulate a car travelling behind a lorry in a rainy day. It is not part of the homologation process, but it is an internal practise of FCA. The facility used is the cold wind tunnel in Orbassano, here the same set of nozzles seen in the experimental test of the previous chapter is used to simulate the wake of a lorry during a rainy day. The nozzles are located in front of the vehicle so that they aim at the air intake system area. The conditions assumed for this test are the following:

- wind speed equal to $V_\infty = 80km/h$
- engine running with wide open throttle
- engine running with 4th gear (wheels are rotating)
- water flow rate is known as well.

The test should last 120 minutes in order to observe the overall amount of water that reaches the engine. As it is easy to imagine (and as will be confirmed in the following sections), the mass flow of water being ingested is constant with respect to time. As a consequence, the test can be shorter. The amount of water registered, then, can be projected in time in order to get the result of ingested water after 120 minutes. Moreover, it is important to monitor the traction load of the car in order to check if the engine is losing power. If a power loss is detected, the test is not successful. Once the test is over, in order to measure how much water has entered the engine intake system, the filter box is opened and the filter is dismounted and weighted. The extra weight found plus the amount of water found in the filter box is assumed to be the overall amount of water that has reached the engine during the test. Of course this method neglects the amount of water that actually overcomes the filter, reaches the engine and gets involved in the combustion. However, for the test to be successful, a specific quantity of water must not be reached. For a 2.4L engine this limit is set equal to:

$$m_{max}[g] \tag{5.1}$$

As said before, the nozzles are the same as used before. This time, though, they are located at a specific location, in particular their position is $1m$ in front of the vehicle and $0.730m$ from the ground.

As far as Jeep Renegade 2.4L Multiair is concerned, its first test was not successful. Therefore, in order to understand how the problem could be fixed, a quick solution was found inserting a shield just before the dirty air duct inlet. The test was then repeated with this new device and its result was successful. This shield prevents most of the water from entering the duct at the same time the engine is still capable of working without losing power (which means that that the right air mass flow is still provided). Hence, water ingestion numerical investigations have to be compared with data from these experimental tests. Therefore, before proceeding with CFD, the shield has to be introduced and integrated within the geometry of the car.

Figure 5.3: Picture of the water spraying system used in the Slipstream test. Courtesy of FCA

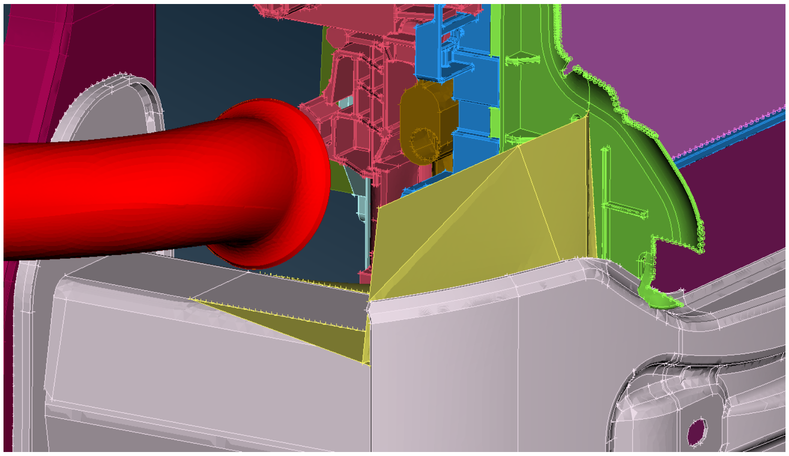

Figure 5.4: Recreated CAD model of the shield mounted on the 2.4L Jeep Renegade to pass the Slipstream test. In particular the red part is the engine intake system dirty air duct, while the shield is coloured with beige.

5.3 Simulation set-up

To set-up the simulation, the Lagrangian Multiphase model is selected. This model is chosen because it is the only one capable of placing a source of Lagrangian parcels in a specific location within the domain (the DMP properties, for example, have to be assigned at the domain inlet). Four sources (or injectors) are located at the real positions of the nozzles in the wind tunnel. In order to better replicate how droplets are sprayed toward the car, a solid cone injectors type is selected. This means that four virtual cones are placed in front of the car. Each of their vertexes is located at the real nozzle coordinates and the cones are oriented toward the engine intake system area, as actually done in the experimental test. The solid cone angles are set equal to 45°. Every parcels is set to be born with the same velocity magnitude as the air has in that point, while its direction is assigned randomly, provided that it stays inside the solid cone. As far as mass flow is concerned, each injector has a mass flow equal to $\frac{\dot{m}_{in}}{4}$. In order to increase the randomness of droplet propagation, the *parcel stream* number n_s has to be increased: this parameter specifies the number of parcels created by every injector at every time-step. A good compromise between the parcel stream number and acceptable run times is found setting this parameter equal to $n_s = 10$. With this value it is possible to calculate the number of parcels (whose diameter is set to be equal to $d_p = 1mm$) carried by each particle. Simply, the mass of a parcel is given by:

$$m_{parcel} = \frac{\frac{\dot{m}_{in}}{4}\Delta t}{n_s} \tag{5.2}$$

where $\Delta t = 0.01s$ is the simulation time-step chosen. It is important to point out that reducing the time-step slows down the whole simulation process for two reasons. The first one is obviously due to a greater number of steps to resolve, while the second one is due to the parcel stream number. If it does not change, the same number of parcels per time-step is always introduced and, as a result of that, a very higher number of parcels is present within the domain after the same time. However, as already mentioned before, the values used for Δt and n_s provide an acceptable compromise. In order to finally estimate the number of particles carried by each parcel (N), the parcel mass found in equation 5.2 is simply divided by the particle mass:

$$m_{particle} = \rho_{water} V_{particle} = \rho_{water} \frac{4}{3}\pi \left(d_p/2\right)^3 \tag{5.3}$$

$$N = \frac{m_{parcel}}{m_{particle}} = 21 \tag{5.4}$$

So 21 particles are carried by each Lagrangian parcel. Moreover, in order to increase the chance of a parcel to reach the intake system, the fluid film model is not activated in these simulations. In fact, parcels are set to interact with boundaries trough elastic collisions, so that they can bounce back and be driven away by the air stream again. In this way the situation is made more critical, since parcels can not stop on any boundary. Moreover, to calculate fluid film on the complex geometry of the under-hood components would be extremely expensive and time consuming. Again, in order to speed up the calculation time, parcels break-ups and and collisions are neglected.

In terms of CFD modelling, the filter is seen as a porous region. This is not the proper way to simulate it, given that only the porous inertial resistance and the porous viscous resistance are assigned (see equation 2.50). In fact the porous medium model provides a governing law between the flow at the inlet and the one at the outlet, but it does not take into account the effects of inside a material that is similar to a sponge. Despite this, though, the porous medium model is the one that gets closer to the real behaviour of the filter.

5.4 Water ingestion: results

5.4.1 Case 1 - 2.4L engine Jeep Renegade

The cumulative amount of water that crosses some interfaces within the two ducts is monitored. In particular these interfaces are placed both in the dirty air duct and in clean air duct at different distances. To do this measurements, the incident mass flux of water is calculated at every time step on the interfaces. This value is then multiplied by the time-step in order to get the net mass that crossed the interface in that time interval. So the overall amount of droplet can then be calculated as:

$$m_{wtot} = \sum_i \left[\Delta t_i \int_A \rho_{water} \mathbf{V}_d \cdot \mathbf{n} dA \right] \tag{5.5}$$

where A is the surface area of the interface, $\mathbf{V}_d$ is the velocity of the parcel and $\mathbf{n}$ is the unit vector normal to the interface. The sum takes into account all the time-steps of the simulation. In order not to spend too much time in computing the solution, the time-step chosen is $\Delta t = 0.01s$ and the overall physical time is set equal to $60s$.

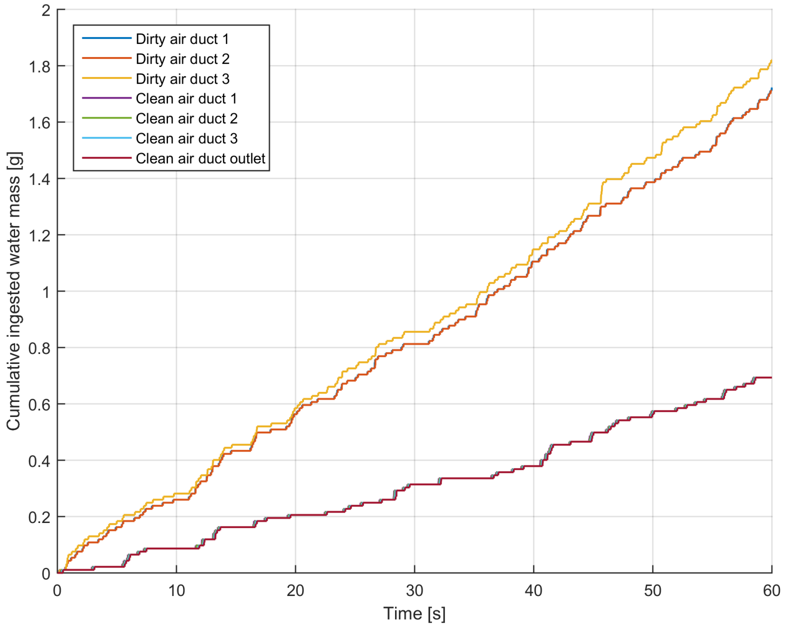

Figure 5.5: Plot of cumulative water mass trough the intake system for 2.4L Jeep Renegade, no shield before the intake.

Figure 5.5 shows the cumulative water mass that crosses the interfaces inside the intake system with respect to time for the first simulation, that is the 2.4L Jeep Renegade with no shield before the intake inlet. It is clear that the trend is linear (as expected), so multiplying the results obtained for one minute by 120 gives the result for two hours, that has to be compared with the experimental one. It is very important to notice that the previous plot shows mainly two different trends: one for the dirty air duct and one for the clean air duct. In fact all the interfaces that belong to one duct give the same cumulative water mass with respect to time (so the lines are almost superimposed in the plot of Figure 5.5). As expected, the amount of water that crosses the clean air duct is lower the that in the dirty air duct. As a consequence of that, the difference between the two results can be seen as the amount of water that remains within the filter, that is what is actually measured after the wind tunnel test. The results are reported by the following table:

	After 120 min
Dirty air duct [g]	1.30x
Clean air duct [g]	0.50x
Filter [g]	0.80x
Experimental [g]	x

Table 5.1: Water ingestion simulation results for 2.4L Jeep Renegade, no shield before the engine intake duct. All the values are referred to the experimental one, whose value is confidential

If modelling a filter as a porous region is considered a valid choice (this fact can be heavily discussed), then the amount water accumulated within the filter after 120 minuted is equal to $0.80x$, while the experimental value is equal to x. This indicates that water trapped within the filter given by CFD simulation is greater than the one found in the wind tunnel test by approximately 20%.

On the other hand, if the porous medium model is not trusted as a way to model an air filter, then the only reliable number is the water mass that entered the intake system: $1.30x$. This value, though, can not be compared with the experimental value. In fact, the experimental result does not takes into account the droplets the travel until the engine cylinders, while the numerical result does. According to what reported in section 5.2, the Slipstream test is not passed if the water mass found within the filter is greater than m_{max} (introduced before, whose value is confidential). Given that the experimental result is negative, the numerical result is expected to be negative as well. For this reason, to trust only the amount of water that reaches the intake system ($1.30x$ in this case) should be the correct procedure. In fact, if the value of $0.80x$ is assumed good, the prediction would be wrong, since the numerical simulation would give a positive result, and the experimental one a negative result. In case this kind of methodology is applied again, then, if the amount of water that reaches the intake system is lower than m_{max}, then the test is likely to be positive, being this way to interpret the results very conservative.

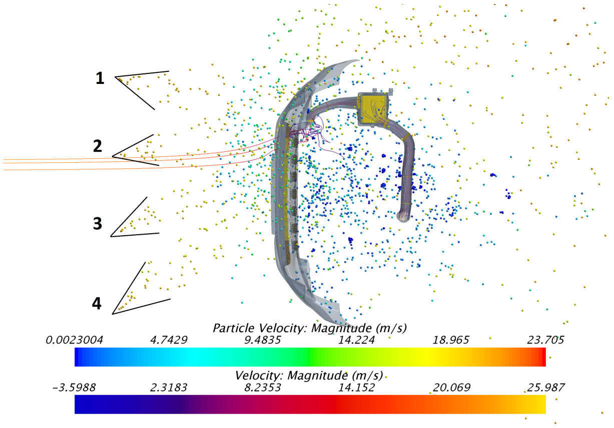

Figure 5.6: Front bumper and grids are shown together with the intake system. The streamlines are generated from the intake system outlet. The four injector cones are clearly visible, as well the particles they generated and their velocity.

5.4.2 Case 2 - 2.4L engine Jeep Renegade with intake shield

The same simulation is now repeated on a different geometry. As done in the experimental test, a shield is inserted before the intake system inlet, as shown by Figure 5.7. In particular, this shield is placed in the gap between the front bumper and the intake system. Of course the purpose of the shield is to prevent water from reaching the intake system, so that a first solution to pass the Slipstream test can be given. In order to increase the accuracy around that area, the mesh is refined around the shield. The injectors for the Lagrangian phase are exactly the same as before, as well their water mass flow and parcel stream numbers.

The following table shows the results for this simulation:

	After 120 min
Dirty air duct [g]	2.98y
Clean air duct [g]	1.71y
Filter [g]	1.27y
Experimental[g]	y

Table 5.2: Water ingestion simulation results for 2.4L Jeep Renegade, a shield is placed before the engine intake duct. All the values are referred to the experimental one, whose value is confidential

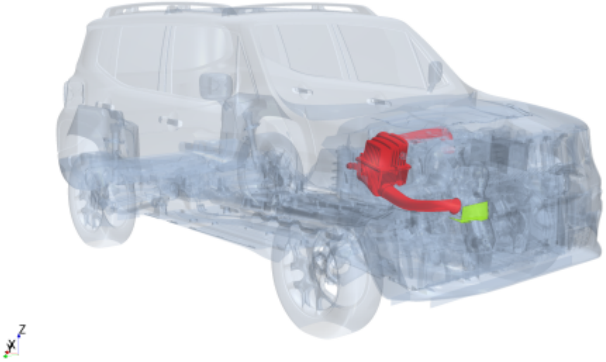

Figure 5.7: Position of the intake system shield. The intake system is coloured in red and the shield is coloured in green.

All the numbers in the table confirm that the test is successful, as it happens in the wind tunnel test. As done before, due to the high level of uncertainty that concerns the filter model, only the amount of water detected into the dirty air duct is considered as a reliable result. Therefore, if a shield is mounted, after two hours the total mass of water that reaches the engine intake system is equal to $2.98y$. If this value is compared with the one from table 5.1, then it is clear that the shield works well. In particular 43% less water enters the system. According to only the experimental data, though, the water mass found within the filter is reduced by 75%. The reason for this difference can be assigned to two main factors:

- A *different shape* of the shield. In fact, no CAD model of that shield is available, since it is only a try done by the wind tunnel operators to provide a quick solution to the problem. So, here the shield is drawn from scratch, with only the pictures of the real one available.

- the *water that overcomes the filter*. As stated before, the wind tunnel test does not take into account the amount of water that actually reaches the engine. This can be another cause of the difference seen between the experimental and numerical deltas. It has to be remembered that the air mass flow does not change since it is imposed at the end of the clean air duct.

The lack of fidelity of the porous medium model used for a filter is again confirmed by a comparison between table 5.5 and 5.7. In fact, if the water trapped within the filter is checked, in the first case it is underrated, while in the second case it is overrated. This difference in these two results is a clear sign that a new and more reliable approach has to be found to model something similar to a sponge.

Chapter 6

Conclusions and future work

In this last Chapter, the conclusions of the thesis are firstly reported, followed by some tips to improve the work done.

6.1 Conclusions

6.1.1 Soiling

As far as water soiling is concerned, several approaches were tested. Both Eulerian and Lagrangian methods were compared and an experimental test was attempted. Table 6.1 sums up all the positive and negative sides of each numerical strategy. Much attention is paid to the computational resources required by each strategy, rather than to the accuracy of the results and their level of fidelity with respect to reality. In fact, as seen in Chapter 4, an accurate prediction for the exterior water management of a vehicle is subject to many degrees of freedom. However, a general behaviour for water that reaches the surface of the car is found. Almost all of the simulations (and the experimental test) agree on the fact that the Jeep Renegade is subject to side glass wetting during a very intense rainy day. In terms of CFD models, the Dispersed Multiphase model is for sure the most reliable one. It is the cheapest one in terms of resources required. Moreover the results provided by the DMP model look very similar to the experimental ones. The Lagrangian Multiphase model, on the other hand, provides similar results, but it takes much more time to get them (more than twice). Moreover it is more difficult to set up: the right balance between the mesh, the number of parcels generated at every time-step and the time-step itself has to be found and it takes several tries to find the right equilibrium. Then, as far as the background flow is concerned, URANS equation with the k-ϵ turbulence model showed to be the right approach. Soiling is phenomenon that takes time to develop and reach a steady state. For this reason the method chosen must allow the computation of several time-steps without requiring too much time or computational resources. URANS equations are the only approach capable of providing a solution in relatively few time.

As far as the proper Soiling investigation is concerned, the side glass of the Jeep Renegade gets wetted when cloudburst conditions are applied. In particular, water falls from the roof on the top-left corner of the side glass and can cause some visibility problems. In fact it spreads on the glass, such that it can obstruct the driver's visibility of the rear view mirror. Despite this though, it has to be remembered that the amount of rain used in the simulations described Chapter 4 is very high (in fact it is associated to a cloudburst). The choice of this kind of rain intensity has two advantages: the first one is to put the car in a critical condition, while the second one is to

Table 6.1: Pros and cons of the different approaches used for Soiling investigation

Multiphase model	**Background flow model**	**Pros**	**Cons**
DMP	URANS (k-ϵ)	Very quick and cheap	Source must be a domain inlet
Hybrid (DMP-Lagrangian)	URANS (k-ϵ)	-	Very slow and doesn't add any information with respect to DMP
Lagrangian	URANS(k-ϵ)	Each parcel can be tracked and there are many customizations	If not well setted can be extremely expensive
DMP	URANS (k-ω)	-	The results are very different from the others
DMP	DES (k-ϵ)	Very accurate	Very sensible to boundary conditions and quite slow

provide a fast phenomenon, so that it can be detected within less physical time, which means less time-steps.

6.1.2 Water ingestion

Differently from what seen for Soiling, water ingestion numerical simulations were run with URANS equations coupled with the Lagrangian multiphase flow. This model is the one capable of placing one or more sources of Lagrangian parcels within the domain, and not, as done by the DMP, on a boundary. This feature is exploited in order to recreate the Slipstream test performed in FCA climatic wind tunnel. Two of these tests were simulated and compared with experimental results. In particular the numerical domain takes into account the engine intake system and all of its components. At the end of this system the engine air mass flow is imposed as boundary condition, while the filter is described as a porous medium. This particular model is found to be the biggest problem. In fact it does not properly takes into account all the phenomena that actually happen within the filter. This is proved by the fact that in one case the numerical simulation overrates the amount of water trapped within the filter with respect to the experimental value, while the second numerical simulation underrates it. As a consequence of that, this approach has to be trusted only for the amount of water detected to enter the intake system. This will be then divided between water that remains in the filter (or falls into the filter box) and water that actually reaches the engine.

As far as the Lagrangian Multiphase model set-up is concerned, again an equilibrium between the first the time-step and the number of parcels generated per time-step has to be found. The parameters reported in Chapter 5 provide a good compromise for this kind of simulation and can be used again on other vehicles, for example. In fact, to numerically predict whether the Slipstream test is passed or not can be an important design criterion during the design/packaging phase of a vehicle. Moreover, as done here, it can be one more way to confirm what done in the wind tunnel.

6.2 Future work

In order to improve the work done here, some steps forward can be made on the soiling investigation. For example the level of randomness of the Lagrangian Multiphase simulation can be increased. One way to do that is to increase the source points and make them alternate faster. Moreover, a particle diameter distribution could also be applied. On the other hand, different rain intensities can be quickly applied to the DMP simulations as different values for the volume fraction. The results obtained would help to understand whether the phenomena seen here happen with different rain intensities too.

As far as water ingestion is concerned, the procedure shown here can be confirmed by doing the same simulations on other vehicles. Since the Lagrangian Multiphase model is applied, here a droplet diameter distribution can be applied as well. The real improvement, though, would be to develop a proper physical model whose purpose is to describe the real behaviour of a spongy material, such as the engine filter.

Bibliography

[1] J.D.Jr Anderson. *Computational Fluid Dynamics - The basics with applications.* McGraw-Hill, 1995.

[2] S. B. Pope. *Turbulent Flows.* Cambridge University Press, 2000.

[3] S.H. Collicott E.L. Houghton, P.W. Carpenter and D.T. Valentine. *Aerodynamics for engineering students, sicth edition.* Elsevier, 2013.

[4] D.C.Wilcox. Formulation of the k-ω turbulence model revisited. *AIAA Journal*, 46:359 – 375, 2011.

[5] CD-Adapco Siemens. *Star-CCM+ 10.06 User Guide.*

[6] M. Hartmann T. Hagemeier and D. Thvenin. Practice of vehicle soiling investigations: A review. *International Journal of Multiphase Flow*, 37(8):860 – 875, 2011.

[7] A. Aroussi S.A.A.A. Ghani and E.Rice. Simulation of road vehicle natural environment in a climatic wind tunnel. *Simulation Practice and Theory*, 8(11), 2008.

[8] I. Spruss J. Jilesen et al. Advances in a-pillar water overflowadvances in a-pillar water overflow. *SAE Technical Paper*, 2015-01-1549, 2015.

[9] A.P. Gaylard and K. Kirwan. Surface contamination of cars: a review. *Proc IMechE Part D: J Automobile Engineering*, 231(9):1160 1176, 2017.

[10] D. Croteau D. Dasarathan, J. Jilesen and R. Ayala. Cfd water management design for a passenger coach with correlation. *SAE Technical Paper*, 2016-01-8155, 2016.